P2.7 Climatology of convective modes for significant severe thunderstorms in the contiguous United States

Bryan T. Smith, Richard L. Thompson, Jeremy S. Grams, and Chris Broyles
Storm Prediction Center
Norman, OK

1. Introduction

Emphasis on convective mode understanding has increased considerably the past few decades, beginning with the initial work by Browning (1964) documenting conventional radar observations and inferred airflow within supercell thunderstorms, continuing with descriptions of organized "bow echoes" (Fujita 1978), and a host of more recent studies (e.g., Weisman and Trapp 2003, Trapp and Weisman 2003) examining quasi-linear convective systems (QLCS). Convective mode is widely recognized as an important contributor to the likelihood and type of severe convective weather (e.g., tornado, large hail, damaging wind gusts). Prior work by Trapp et al. (2005; hereafter T05) considered a relatively simple designation of convective mode for all tornadoes in the continental United States for 1999-2001. They used regional radar mosaics of base-elevation radar reflectivity, and did not attempt to specify convective mode beyond a QLCS, cell, or "other" classification scheme, as did Thompson et al. (2008). Gallus et al. (2008) employed a more detailed radar reflectivity classification scheme (nine distinct convective morphologies). Like T05, Gallus et al. (2008) examined regional radar reflectivity mosaics every 30 minutes, and associated all severe reports with a storm type over the Great Plains and Upper Midwest states during the 2002 warm season. More recent work by Duda and Gallus (2010) considered the same nine convective morphologies and geographic region as Gallus et al. (2008), except for the 2007 warm season and with the addition of supercell identification based on explicit output from the mesocyclone detection algorithm (MDA) described by Stumpf et al. (1998). Their supercell identifications relied on consecutive volume scans of the MDA output, requiring a cellular convective morphology.

**Corresponding author address:* Bryan T. Smith, NOAA/NWS/NCEP/Storm Prediction Center, 120 David L. Boren Blvd., Suite 2300, Norman, OK 73072. Bryan.Smith@noaa.gov

The aforementioned studies dealt with classification schemes, some of which were relatively simple, based primarily on radar reflectivity mosaics with rather coarse spatial and temporal (30 min) resolution. Weather Surveillance Radar-1988 Doppler (WSR-88D) data began to be archived in the early to mid 1990s (Crum et al. 1993) and, until recently, detailed individual radar convective mode climatologies have not been possible. Studies such as Hocker and Basara (2008a,b) and Smith et al. (2008) utilized full WSR-88D volumetric data (base reflectivity and base velocity at multiple elevation scans updated every 5 minutes), but for only state or regional investigations of convective mode and resultant spatial/temporal evolutions of supercells or QLCS. This study incorporates various strengths of past convective mode investigations such as increasing the number of radar recognizable storm classifications (e.g., Gallus et al. 2008, Duda and Gallus 2010) via volumetric WSR-88D level II data for a large sample of severe thunderstorm and tornado events. Following Hales (1988), we focus our efforts on tornadoes and significant severe reports (i.e., 2"+ diameter hail (hereafter sighail) and 65+ kt convective wind gusts (hereafter sigwind)) since they often result in a disproportionate threat to life and property.

In the following section, our data collection methodology is detailed and associated challenges with radar-based subjective analysis of storm mode classification are discussed. Section 3 features severe event distribution across various convective modes and seasons, and an estimated spatial distribution across the contiguous U.S. Section 4 includes a summary discussion and outline of future work related to the Storm Prediction Center (SPC) convective database. A continuing portion of this study (Thompson et al. 2010, this volume) examines relationships between severe reports, convective mode, and environmental data using SPC hourly mesoanalysis data (Bothwell et al. 2002; Schneider and Dean 2008).

2. Data and methodology

a. Data and event filtering

All tornado, sighail and sigwind reports for the period 2003-2009 were filtered for the largest magnitude report per hour on 40 x 40 km RUC model (Benjamin et al. 2004) analysis grid (Fig. 1). Tornado segment data were used in order to provide slightly higher tornado damage intensity resolution. This filtering procedure produced a sample of 17037 severe thunderstorm grid-hour events, including 8176 tornadoes (78% of all tornadoes), 3361 sighail (80% of all sighail), and 5500 sigwind (82% of all sigwind) during the seven year period. We did not consider sub-significant hail/wind events or null cases (i.e., storms without severe weather reports) due to the difficulty of case identification associated with the overwhelming sample size.

Numerous studies have highlighted apparent weaknesses in severe convective wind reports in the National Climatic Data Center (NCDC) publication *Storm Data.* Some of these include: overestimated wind speeds by human observers (Doswell et al. 2005), a largely secular (non-meteorological) increase in the number of reports (Weiss et al. 2002), and the dependence of report frequencies on population density and time of day (Trapp et al. 2006). Similar issues impact tornado reports (e.g., Doswell and Burgess 1988). These caveats associated with the severe report database are acknowledged but accepted for purposes of this study. With the above limitations in mind, the authors made careful adjustments to a small portion (4.5%) of the database. A large majority of suspected report errors involved incorrectly listed report times when event times were compared to radar data. Examples of this suspected error type included reports well removed from existing convection and time differences on the order of tens of minutes to an hour or more. Offsets of one hour were relatively common near time zone boundaries, though a few reports required extensive investigation to identify errors of up to several days. In situations where a suspected error could not be easily corrected, *Storm Data* was used to examine the questionable report's description in an effort to identify the storm responsible for the event.

b. Radar-based storm mode classification criteria

Archived level II WSR-88D data from NCDC (http://www.ncdc.noaa.gov/nexradinv/) were utilized from the closest site[1] (up to 230 km) to assign one of the following major convective mode classes for each severe thunderstorm event: QLCS, supercell (right-moving (RM) or left-moving (LM)), and "disorganized" (cells and clusters clearly not meeting QLCS or supercell criteria) listed below. Sub-classifications of each major category were as follows: QLCS included bow echo; supercell included discrete cell, cell in cluster, and cell in line (examples depicted in Fig. 2); disorganized included discrete cell, cell in cluster, and cluster. Additionally, two other classifications were noted: storms with marginal supercell characteristics (after Thompson et al. 2003), and so-called linear hybrid modes with a mix of QLCS and line RM characteristics (see later discussion in Section 2d). A translation of the convective morphologies presented in Fig. 2 of Gallus et al. (2008) to our classification scheme is as follows (Gallus et al. in parentheses): discrete cell (isolated cell), cell in cluster (cell cluster), cell in line (broken line, length scale dependent), QLCS with bow echo as a subset (five linear modes), and cluster (NL). Our convective mode categories can also be simplified to match T05, where their "other" category includes our disorganized storm cells and clusters.

Our subjective reflectivity threshold for storm identification was 35 dbZ, with QLCS events consisting of contiguous reflectivity at or above the threshold for a horizontal distance of at least 100 km and a length-to-width aspect ratio of at least 3 to 1 at the time of the event, similar to T05 and Grams et al. (2006). Cells were discrete areas of above-threshold reflectivity, and clusters were conglomerates of storms not meeting either cell or QLCS criteria. The Gibson Ridge radar viewers (GRLevel2 and GRLevel3) were used to analyze archived WSR-88D level-II or level-III single site radar data. Convective mode was determined using the volume scan immediately prior to reported severe event time with primary emphasis on the lowest elevation tilt (i.e., 0.5 degrees) of base reflectivity and velocity data for classifying storms; secondary emphasis was then given to subsequent higher tilts of radar data if the lowest tilt was unavailable (e.g., range folded or improperly dealiased velocity data). If level II data were unavailable, then level III data were used. In situations when radar data were unavailable or

[1] Level III archived data were used when level II data were missing, or when a site with only level III archived data provided superior resolution of an event due to horizontal range limitations.

incomplete, convective mode was not assessed (0.37% of total cases).

Discrete or embedded cells with focused areas of cyclonic (or anticyclonic) azimuthal shear were further scrutinized as potential supercells, following the mesocyclone nomograms developed by the Warning Decision Training Branch of the National Weather Service (after Andra 1997 and Stumpf et al. 1998). Supercells required a peak rotational velocity ≥ 10 m s^{-1} (i.e., a peak-to-peak azimuthal velocity difference of roughly 20 m s^{-1} over a distance of less than 10 km). Range dependence was included in the mesocyclone designation, per the 1, 2, and 3.5 nm mesocyclone nomograms. Circulations were classified as weak shear (non-supercell), and weak, moderate, or strong supercells, following a subjective 3-bin ranking of range-dependent horizontal peak rotational velocity guidelines.

c. Spatial event distribution and grid smoothing

Although this dataset includes thousands of event types by convective mode, our sample is necessarily incomplete, and perhaps unrepresentative of a much longer period of time, since it covers only seven years. A spatial smoother was employed to account for likely shortcomings in our sampling of severe storm events, and to provide a preliminary climatological estimate of severe event and convective mode distributions. A kernel density estimation tool using ESRI ArcGIS ArcMap Spatial Analyst extension software was utilized to examine convective mode by event type on a 40 km horizontal grid with a 400 km radius. For the sake of consistency, all kernel density estimates used herein matched the horizontal grid resolution (i.e., 40 km) used for environment assessment (see Thompson et al. 2010, this volume). The kernel function chosen is based on the quadratic kernel function described in Silverman (1986, p. 76, equation 4.5), though it is acknowledged that it may be appropriate to examine other smoothing criteria. For a more thorough discussion on the subjectivity of proper spatial smoothing, refer to Brooks et al. (2003).

d. Mode classification difficulties and challenges

A considerable number of events, particularly in the cool season, featured mixed mode or evolutions from one mode to another (e.g., line RM to QLCS) during the course of a series of events. These cases illustrate the complexity that can occur close in time and space. Figs. 2 and 3 from the 15 November 2005 tornado outbreak show a snapshot view of different convective modes ranging from an F4 discrete RM, cluster RM, tornadic line RM, and finally upscale to a tornadic QLCS across the Lower Ohio and Tennessee Valleys. Arguably more complicated storm evolutions existed (Figs. 4 and 5) in the latter stages of an initial discrete cell that acquired supercell rotation as a cluster RM on 24 August 2006 in central North Dakota. The RM was subsequently overtaken by a developing and eastward moving QLCS that became a bow echo after ingesting the decaying RM. The bow echo comma head circulation resulted in a F2 tornado and sigwind event. Meanwhile, approximately 80 km to the southeast in relatively close proximity in space and time to the bow echo, a predominately discrete RM transitioned to a cluster RM and produced an F0 tornado. This case is just one of many that illustrate the variability in different storm modes in close proximity to one another.

A number of challenges were encountered in the process of identifying convective modes with severe thunderstorm and tornado events. Unambiguous discrimination between clusters and lines, as well as closely-spaced cells versus clusters, was not always possible. The most difficult challenge involved discrimination between QLCS and line RM. Many cases exhibited a mix of RM and QLCS structures, such that a single mode designation was not easily possible (Figs. 6-8). Cases such as this were noted as linear hybrids, after multiple examinations by the authors and other established experts[2] in radar interpretation.

Specific problems revolved around identification of mesocyclones versus "mesovortices" in the linear convective systems. A typical mesocyclone extends through a substantial fraction of storm depth (Doswell and Burgess 1993), whereas QLCS mesovortices are relatively shallow and not clearly associated with other supercell structures (Trapp and Weisman 2003, Weisman and Trapp 2003). When differences between the circulation types were not clear after considering all volumetric radar data, including reflectivity structures like hook echoes, echo overhang, etc.,

[2] The authors express their gratitude to Les Lemon, Jim LaDue, and Paul Schlatter of the Warning Decision Training Branch for reviewing and discussing our radar interpretation for several difficult convective mode cases.

after Lemon (1977), a case was labeled a linear hybrid. The linear hybrid cases were noted in the sample, though each was ultimately assigned either a line RM or QLCS designation, such that the linear hybrids were not a unique classification. This storm mode taxonomic exercise required the authors to address the problem of classifying data that do not necessarily always fit cleanly into a particular "bin".

A very difficult case highlighting this problem (Figs. 6-8) occurred during the early morning hours of 11 May 2008 across central and southeastern Georgia. An initial large cluster of storms moving from Alabama into west central Georgia included several cellular structures ahead of an east-southeastward moving band of storms growing upscale into a QLCS. Storm mergers and complex interactions occurred across central Georgia as the QLCS surged southeastward over the next few hours, and this complex evolution served as a classic illustration of the "gray area" that can exist between line RM and QLCS. Full volumetric radar data were utilized in order to examine the vertical structure and continuity of features needed to differentiate between the line RM and QLCS mesovortices that were responsible for a swath of tornado and sigwind events. The development and continuation of features (e.g., circulations, deep echo overhang and shape, echo tops) aided in mode assessment. The linear hybrid designation also acted as a descriptor to exemplify the uncertainty involved in classifying these cases. Thompson et al. (2010, this volume) provides a detailed examination of characteristics of the near-storm environment associated with the line RM and QLCS convective modes.

Other classification challenges revolved around storm size and ability of the WSR-88D data to resolve supercell structures. Storm depth and rotation were quite shallow in some tropical cyclone and cool season events compared to larger spatial dimensions of storms in warm season Great Plains events. In some cases, rotation and storm depth did not exceed 3000 ft and 20000 ft AGL, respectively. Due to the weaker rotational velocities observed with a small number of these cases, they were at times designated as marginal supercell, which may be partially caused by the inability of the radar to resolve sufficient storm scale rotation (e.g., horizontal range limitations) typical of a supercell per the nomograms used in this study.

e. Storm evolution

Animation of multiple volumetric radar scans was needed in some instances to differentiate between subtle differences when several convective modes (e.g., QLCS and line RM) were in close proximity in time and space (i.e., $\leq$ 10 km and 5 minutes, respectively) to one another. This required intensive radar interrogation that in some cases was not sufficiently unambiguous to classify the event. In those few circumstances, the authors relied upon tracking observable features (e.g., mesocyclones) in the merged reflectivity and velocity data. An overwhelming majority of these cases were initial discrete RM or cluster RM being overtaken by a QLCS and moving in concert with the forward motion of the QLCS. A relatively large portion of these cases continued to exhibit RM characteristics after storm merger, with embedded mesocyclones maintained before the eventual demise of cellular structure. Variability existed in how long a line RM would survive within a larger QLCS, ranging from a few minutes to 30 minutes or more. Given the highly variable nature of line RM demise in merger cases, an arbitrary cutoff of 15 minutes was applied, unless other evidence supported the feature responsible for the reported event. Echo top trends and deeper reflectivity cores aided in this assessment.

Other situations involved transient deeper reflectivity cores within a QLCS that evolved into line RM. This seemed to be most common across the Lower Mississippi Valley during the cool season. One example of this is a tornado and sigwind event over central Mississippi on 10 December 2008. A cursory glance at lowest tilt of base reflectivity from the Jackson, MS (KDGX) radar shows seemingly innocuous QLCS structure around the time of tornado and sigwind events (Fig. 9). Examination of higher tilts of reflectivity and velocity show a deep mesocyclone within a substantially deeper reflectivity core, along with higher echo tops (Figs. 10-12). This case demonstrates the subtlety of proper convective mode classification.

3. Results

Tornadoes were much more common with discrete and cluster RM compared to QLCS and disorganized modes, and sighail events were produced almost exclusively by RM and LM (see Table 1). Conversely, sigwind events were more evenly distributed amongst supercells, QLCS, and disorganized convective modes. Thus, without consideration of environmental information,

sigwind clearly presents the greatest challenge to forecasters given the wide variety of convective modes capable of producing these events. A more detailed look at the tornado events reveal that discrete and cluster RM are most commonly associated with the significant (F2+ damage) tornadoes (Table 2), while 98-100% of the F3+ tornadoes were produced by some form of supercell. Like T05, we found that F1 tornadoes were a little more common with QLCS than F0, and based on their statistical arguments, it appears that F0 QLCS tornadoes may still be under-reported.

All RM tornado events were accompanied by categorical estimates of mesocyclone strength. Weak mesocyclones were most common with weak (F0-F1) tornadoes (Table 3), while F3+ tornadoes were associated almost exclusively with strong mesocyclones. The relative frequencies of mesocyclone strength by F-scale varied little across the three classes of RM (not shown), even though discrete and cluster RM tornadoes outnumbered line RM tornadoes by roughly a factor of 3 to 1.

Caution should be noted in interpreting spatial estimation details near the edges of the domain that are presented next. Some slight underestimate of values within these regions is due to the lack of data over adjacent coastal waters and Canada/Mexico. Additionally, care should be taken in interpreting patterns in locations where only a small number of events control the resulting smoothing estimate. Because there was no sample size filter applied to the kernel density estimates, the most plausible patterns likely exist in areas away from the edge of the domain that also have high numbers of events. With the above considerations in mind, some seemingly robust spatial signals in the relationship between tornado events and convective mode are revealed.

a. Tornado relative frequency by mode

The kernel density estimate provides a smooth field of the event and mode occurrence on the 40 km analysis grid, but it does not explicitly state anything about the absolute occurrence of tornadoes. For example, the relative frequency of discrete RM is higher in northeast Wyoming than southwest Kansas (Fig. 13), but the overall count of tornadoes is much higher in Kansas. Given the occurrence of a tornado in northeast Wyoming, Fig. 13 suggests a slightly higher probability of a discrete RM compared to southwest Kansas. The absolute rate of occurrence of discrete RM tornado events is actually higher in Kansas than Wyoming, though the relative frequency of discrete RM tornadoes in Kansas is reduced due to large numbers of tornadoes from other convective modes. At least 40% of all tornadoes occurred with discrete RM across a sizable portion of the southern and central High Plains. The higher relative frequencies of discrete RM in areas such as northern Maine, western Montana, and southern Nevada are sensitive to small sample sizes and may not be representative of the longer term climatology. The aforementioned caveats also apply to Figs. 14-19.

The discrete RM tornado events were most common in the High Plains with a slight eastward shift and lower relative frequency for cluster RM (Fig. 14) in the central and eastern Great Plains. A relative minimum corridor is noted in the Lower Mississippi and Ohio Valleys which corresponds to a higher relative frequency of line RM (Fig. 15) in the Lower Mississippi and Tennessee Valleys and QLCS across the Ohio Valley (Fig. 16). A sum of the discrete and cluster RM (not shown) yields a pronounced bi-modal spatial distribution with a maximum relative frequency of tornado events (in excess of 80%) centered over western Oklahoma. A sum of the line RM and QLCS is shown in Fig. 17 and illustrates the distinct tendency for tornadoes with linear convective modes in the Lower Mississippi Valley northward to the Ohio Valley. Tornado events were dominated by all RM (Fig. 18) across the Plains and Southeast, with RM contributing less to tornado event frequencies in the Ohio Valley and southern Great Lakes. Tornado events with disorganized cells or clusters (Fig. 19) were relatively uncommon across the same areas dominated by supercells, except for parts of the Upper Midwest, eastern Colorado (i.e., the Denver Convergence Vorticity Zone described in Brady and Szoke 1989), and the Florida peninsula largely attributable to diurnal sea breeze thunderstorms and boundary interactions during the summer (Collins et al. 2000).

b. Seasonal spatial distribution by mode

Tornado events with discrete and cluster RM clearly peak in May (Fig. 20), with a secondary peak in September related to tropical cyclones (Edwards 2010, this volume). The linear convective modes (QLCS and line RM) also peak in the spring and decrease rapidly from May to July, though at a substantially reduced rate of

occurrence compared to the discrete and cluster RM tornadoes. Tornadoes with disorganized convective modes (discrete non-supercellular storms and clusters) reach a maximum during the summer (June-July), with very few events during the winter. Though the winter frequencies of tornado events pale in comparison to the spring, tornadoes with linear convective modes were nearly as frequent as discrete or cluster RM (Fig. 21). The discrete and cluster RM account for roughly 50-65% of all tornadoes events throughout the year, whereas the linear convective modes approach a relative frequency near 50% only during the winter. May appears to be the most consistent time of year for supercell tornadoes. The monthly distribution of tornado events suggests greater predictability may be possible in May as a result of decreasing relative frequencies of QLCS tornadoes compared to the winter months, and prior to the upswing in disorganized convective modes in the summer. However, a thorough evaluation of predictability in May would require a comprehensive sample of nontornadic supercells. A similar relative maximum in discrete and cluster RM occurs in September, though this secondary maximum is related to tropical cyclone landfalls (Edwards 2010, this volume) as opposed to the more common "synoptically evident" (Doswell et al.1993) severe weather scenarios in May.

The kernel density estimates shown in Fig. 22 highlight the degree of spatial clustering for RM tornadoes by season. The absolute tornado counts vary substantially by season, with many more tornado events in the spring (Fig. 22, top right) compared to the winter (Fig. 22, top left). The cluster centroids (i.e., the orange/red shaded areas within the estimated 25th and 10th percentile contours) represent the *relative density of events by season*, and should not be confused with the actual density of events comparing one season to another. RM tornado events were most common across the interior northern Gulf Coast during the winter, with the most frequent areas shifting northwestward into the central Plains during the spring, northward into the northern Plains and Midwest during the summer, and then back southward into the Lower Mississippi Valley during the fall. During the late summer and early fall, a secondary maximum corridor is evident across the Mid-Atlantic and Southeast largely attributed to multiple tropical cyclone tornado events in 2004 and 2005 (Edwards 2010, this volume). The significant tornado events (F2-F5 damage) with all RM (Fig. 23) show a similar seasonal distribution when compared to all tornadoes, except for the northward shift from the Lower Mississippi Valley toward the Lower Ohio Valley in the fall.

The QLCS tornado events displayed a notable eastward shift away from the Plains toward the Mississippi and Ohio Valleys (Fig. 24), compared to RM during the spring and summer. The distributions of disorganized tornado events (Fig. 25) vary substantially from both the RM and QLCS tornado events by season. Local maxima in relative frequency are apparent across central California during the winter, as well as eastern Colorado and the Upper Midwest during both the spring and summer. The relative frequency of disorganized convective modes is also large across Florida in the summer, where diurnal convection is common with local sea breeze circulations. Many of the disorganized mode tornado events along the Gulf Coast in the fall were related to tropical cyclone landfalls, when supercell structures were not apparent with some cellular storms.

As seen in Table 1, the vast majority of sighail events occurred primarily with discrete and cluster RM and LM. The sighail events show a clear preference for the Plains during the spring and summer (Fig. 26), with the greatest frequency of sighail events displaced to the south of the maxima in RM tornado events (Fig. 22) for the same seasons. The fall sighail distribution also favors the Plains compared to the Lower Mississippi Valley for RM tornadoes, but the sample size for fall sighail events is smaller by an order of magnitude and confined largely to September.

Sigwind events with RM (Fig. 27) were distributed similarly to RM tornadoes (Fig. 22) during the winter, spring, and summer. The most noteworthy differences occur in the fall, with the sigwind RM events occurring spatially between the early fall sighail event distribution in the Plains, and the late fall RM tornadoes across the lower Mississippi Valley. Unlike the RM tornadoes, there is little evidence in the sigwind event data of a secondary relative maximum in the late summer and early fall from Georgia to the Mid-Atlantic. QLCS sigwind events (Fig. 28) occurred along more of a north-south corridor from the Lower Mississippi Valley to the Ohio Valley in the winter and fall, compared to a more east-west corridor for RM tornadoes (Fig. 22) in the winter and fall across the interior Gulf Coast The summer QLCS sigwind events were displaced slightly southeastward over northern

Illinois extending southeastward towards the Ohio River, similar to the northwest flow pattern for severe weather outbreaks depicted in Johns (1984) that occurs in the summer across the northern Plains to the Midwest.

The disorganized sigwind events (Fig. 29) were concentrated in late spring and summer from the central Plains eastward to the southern Appalachians, with a relative minimum within this corridor across the Mississippi Valley. The southern Appalachians relative maximum represents a substantial shift farther southeast than the RM and QLCS sigwind events (Figs. 26-28) in the Midwest. Interestingly, the disorganized sigwind events appear to be uncommon across the Gulf Coast and Florida in the summer, despite the high frequency of diurnal thunderstorms. This is likely related to the infrequency of reported wind gusts $\geq$65 kt produced by collapsing pulse storms. The clusters of events near Phoenix and Tucson, Arizona and Salt Lake City, Utah in the summer are likely related to local topography and increased density in population and/or observing systems compared to the other sparsely populated areas of the Intermountain West. Small sample sizes preclude any substantial conclusions regarding the winter and fall sigwind distributions.

c. Temporal distribution of tornado events by radar site

Tornado events within 230 km of the two WSR-88D sites exhibiting the greatest overall frequency of tornadoes in our sample (Dodge City, Kansas (KDDC) and Jackson, Mississippi (KDGX)) were chosen to examine the diurnal distribution of events with the three primary tornadic modes (RM, QLCS, and disorganized). Tornado events were dominated by RM at KDDC (Fig. 30), with a classic Plains temporal distribution from 2200 to 0300 UTC (late afternoon through late evening). Tornadoes with QLCS or disorganized modes were much less common than RM tornadoes, but still tended to occur during the same portion of the day as the RM tornadoes. Conversely, KDGX (Fig. 31) reveals a much different distribution of tornado events by mode. Tornadoes with RM occurred throughout the day and night, with more muted peaks around late afternoon and during the early morning hours. QLCS tornado events were much more common than at KDDC, and these QLCS events were distributed throughout the overnight and morning hours, with a pronounced minimum during late afternoon. Tornadoes with disorganized storms were rare within the coverage envelope of the KDGX radar site. These two sites represent only a small fraction of all tornado events across the contiguous United States, but Figs. 30 and 31 illustrate the potential for the development of convective mode climatologies for various radar sites.

4. Summary

Single-site, volumetric WSR-88D level II data were utilized to assign a convective mode for nearly 17000 tornado, sighail , and sigwind events, representing around 80% of all such reported occurrences across the contiguous U.S. from 2003-2009. Four primary categories of mode classification included: QLCS, RM and LM supercells, and disorganized. Sub-classifications were also assigned: bow echo, discrete cell, cell in cluster, cell in line, cluster, marginal supercell, and linear hybrid. Many event cases were very difficult to classify due to convective mode transitions and presented many challenges in trying to "bin" convective mode across a spectrum of storm types. A considerable number of events featured mixed modes, or evolutions from one mode to another (e.g., line RM to QLCS), during a sequence of severe weather events. The most difficult challenge involved discrimination between QLCS and line RM. Many cases exhibited a mix of RM and QLCS structures, and such cases were noted as linear hybrids to convey a level of uncertainty in classification.

Although various degrees of uncertainty existed in subjectively classifying a convective mode, especially those with complex storm-scale evolutions that occur near the time of a given report, the sheer number of cases likely overwhelms the uncertainty associated with any specific event mode designation. As such, the relative frequency, along with spatial and temporal distributions, illustrate important differences that convective mode has on the type of severe weather.

The majority of tornadoes occurred with discrete and cluster RM compared to QLCS and disorganized modes, with this tendency increasingly common as the F-scale damage ratings increased. Similarly, weak mesocyclones were most common with weak tornadoes, while F3-F5 tornadoes were associated with strong mesocyclones around 90% of the time. At least 95% of F3-F5 tornadoes and sighail events were produced by supercells. Conversely, sigwind events were more evenly distributed amongst RM,

QLCS, and disorganized convective modes. Thus, without consideration of environmental information, significant wind events clearly present the greatest challenge to forecasters given the wide variety of associated convective modes.

Kernel density estimation was performed on a 40 km analysis grid to depict the spatial and seasonal distribution of event types by convective mode. Higher relative frequencies of discrete RM occurred across the High Plains, with a slight eastward shift to the central and eastern Great Plains for cluster RM tornado events. Higher relative frequencies of line RM tornado events occurred in the Lower Mississippi and Tennessee Valleys, while QLCS tornado occurrence was relatively greater across the Ohio Valley. Tornado events were dominated by all RM across the Plains and Southeast, with RM contributing less to tornado event frequencies in the Ohio Valley due to a higher proportion of QLCS tornado events. Tornado events with disorganized cells or clusters were relatively uncommon across many of the same areas dominated by supercells.

A monthly and seasonal breakdown revealed that tornado events with discrete and cluster RM clearly peaked in May, with a secondary peak in September related to tropical cyclones. The linear convective modes of QLCS and line RM also peaked in the spring and decreased rapidly from May to July. Tornadoes with disorganized convective modes (discrete non-supercells and clusters) reached a maximum during June and July, with very few events during the winter. Although the winter frequency of tornado events was substantially less than spring, tornadoes with linear convective modes were nearly as frequent as discrete or cluster RM. From a forecasting perspective, this implies that May potentially can be a more predictable time of year for supercell tornadoes as a result of decreasing relative frequencies of QLCS tornadoes compared to winter and prior to increasing relative frequencies of disorganized convective modes in the summer.

RM tornado events were most common across the interior northern Gulf Coast during the winter, with the most frequent areas shifting northwestward into the central Plains during the spring, northward into the northern Plains and Midwest during the summer, and then back southward into the Lower Mississippi Valley during the fall. Conversely, QLCS tornado events displayed a notable eastward displacement away from the Plains toward the Mississippi and Ohio Valleys during the spring and summer. Supercell sighail events were clearly most common across the Plains during the spring and summer. Sigwind events with RM were distributed similarly to RM tornadoes during the winter, spring, and summer.

QLCS sigwind events were common along more of a north-south corridor from the Lower Mississippi Valley to the Ohio Valley in the winter and fall, compared to an east-west corridor for RM tornadoes in the winter and fall across the interior Gulf Coast. Spring QLCS sigwind events were more common slightly to the east and northeast of the spring RM tornadoes, and somewhat to the southeast of the spring QLCS tornadoes. The summer QLCS sigwind events aligned generally along the previously documented corridor of northwest flow severe weather outbreaks across the Midwest.

Future work will include continued expansion of the database on a yearly basis, with the goal of providing a solid foundation for multi-faceted forecast verification at the SPC. As the dataset expands, the examination of diurnal trends for various convective modes by severe type using a defined time period (e.g., hour, month) will be possible. A unified community convective mode classification scheme is sorely needed in order to uniformly describe the full spectrum of storm types, such that classification differences do not overly influence signals in related atmospheric variables (i.e., some of the QLCS designations in Kis and Straka 2010) that would fall in the discrete RM category in this work).

ACKNOWLEDGEMENTS

Andy Dean (SPC) and Jason Levit (Aviation Weather Center) provided assistance in the display and filtering of both radar data and severe events. This work also benefitted from multiple discussions with Steven Weiss and Dr. Russell Schneider (SPC), as well as Dr. Harold Brooks (National Severe Storms Laboratory).

REFERENCES

Andra, D. L., 1997: The origin and evolution of the WSR-88D mesocyclone recognition nomogram. Preprints, *28th Conf. on Radar Meteor*., Austin, TX, Amer. Meteor. Soc., 364–365.

Benjamin, S. G., and Coauthors, 2004: An hourly assimilation-forecast cycle: The RUC. *Mon. Wea. Rev*., **32**, 495-518.

Bothwell, P. D., J. A. Hart, and R. L. Thompson, 2002: An integrated three-dimensional objective analysis scheme in use at the Storm Prediction Center. Preprints, *21st Conf. on Severe Local Storms*, San Antonio, TX, Amer. Meteor. Soc., J117–J120.

Brady, R. H., and E. J. Szoke, 1989: A case study of nonmesocyclone tornado development in northeast Colorado: similarities to waterspout formation. *Mon. Wea. Rev.*, **117**, 843-856.

Brooks, H. E., C. A. Doswell III, and M. P. Kay, 2003: Climatological estimates for local daily tornado probability for the United States. *Wea. Forecasting*, **18**, 626-640.

Browning, K. A., 1964: Airflow and precipitation trajectories within severe local storms which travel to the right of the winds. *J. Atmos. Sci.,* **21,** 634–639.

Collins, W. G., C. H. Paxton, and J. H. Golden, 2000: The 12 July 1995 Pinellas County, Florida, tornado/waterspout. *Wea. Forecasting*, **15**, 122-134.

Crum, T. D., R. L. Alberty, and D. W. Burgess, 1993: Recording, archiving, and using WSR-88D data. *Bull. Amer. Meteor. Soc*., **74**, 645-653.

Doswell, C. A. III, and D. W. Burgess, 1988: On some issues of United States tornado climatology. *Mon. Wea. Rev.*, **116**, 495-501.

_____, and _____, 1993: Tornadoes and tornadic storms: A review of conceptual models. The Tornado: Its Structure, Dynamics, Prediction, and Hazards. *Geophys. Monogr.,* **79**, Amer. Geophys. Union, 161-172.

_____, S. J. Weiss, and R. H. Johns, 1993: Tornado forecasting – a review. The Tornado: Its Structure, Dynamics, Prediction, and Hazards. *Geophys. Mongr.*, **79**, Amer. Geophys. Union, 557-571.

_____, H.E. Brooks, and M.P. Kay, 2005: Climatological estimates of daily nontornadic severe thunderstorm probability for the United States. *Wea. Forecasting*, **20**, 577-595.

Duda, J. D., and W. A. Gallus, Jr., 2010: Spring and summer Midwestern severe weather reports in supercells compared to other morphologies. *Wea. Forecasting*, **25**, 190-206.

Edwards, R., A. R. Dean, R. L. Thompson, and B. T. Smith, 2010: Objective environmental analyses and convective modes for U. S. tropical cyclone tornadoes from 2003–2008. Preprints, *25th Conf. Severe Local Storms*, Denver, CO, Amer. Meteor. Soc., P3.2.

Fujita, T. T., 1978: Manual of downburst identification for project NIMROD. Satellite and Mesometeorology Res. Pap. No. 156, University of Chicago, Dept. of Geophysical Sciences, pp. 104.

Gallus, W. A., N. A. Snook, and E. V. Johnson, 2008: Spring and summer severe weather reports over the Midwest as a function of convective mode: A preliminary study. *Wea. Forecasting*, **23**, 101–113.

Grams, J. S., W. A. Gallus, Jr., S. E. Koch, L. S. Wharton, A. Loughe, and E. E. Ebert, 2006: The use of a modified Ebert-McBride technique to evaluate mesoscale model QPF as a function of convective system morphology during IHOP 2002. *Wea. Forecasting*, **21**, 288–306.

Hales, J. E. Jr., 1988: Improving the watch/warning program through use of significant event data. Preprints, *15th Conf. on Severe Local Storms*, Baltimore, MD, Amer. Meteor. Soc., 165-168.

Hocker, J. E. and J. B. Basara, 2008a: A Geographic Information Systems–based analysis of supercells across Oklahoma from 1994 to 2003. *J. Appl. Meteor. Climo*., **47**, 1518–1538.

_____, and _____, 2008b: A 10-year spatial climatology of squall line storms across Oklahoma. *Int'l J. of Climo*., **28**, 765-775.

Johns, R. H., 1984: A Synoptic Climatology of Northwest-Flow Severe Weather Outbreaks. Part II: Meteorological Parameters and Synoptic Patterns. *Mon. Wea. Rev.*, **112**, 449–464.

Kis, A. K. and J. M. Straka, 2010: Nocturnal tornado climatology. *Wea. Forecasting*, **25**, 545-561.

Lemon, L. R., 1977: New severe thunderstorm radar identification techniques and warning

criteria: A preliminary report. NOAA Tech. Memo. NWS NSSFC-1, 60 pp.

Schneider, R. S., and A. R. Dean, 2008: A comprehensive 5-year severe storm environment climatology for the continental United States. Preprints, *24th Conf. Severe Local Storms*, Savannah GA., Amer. Meteor. Soc., 16A.4.

Silverman, B.W., 1986: Density Estimation for Statistics and Data Analysis. New York: Chapman and Hall, pp. 177.

Smith, B. T., J. L. Guyer, and A. R. Dean, 2008: The climatology, convective mode, and mesoscale environment of cool season severe thunderstorms in the Ohio and Tennessee Valleys, 1995-2006. Preprints, *24th Conf. Severe Local Storms*, Savannah GA., Amer. Meteor. Soc., 13B.7

Stumpf, G. J., A. Witt, E. D. Mitchell, P. L. Spencer, J.T. Johnson, M. D. Eilts, K. W. Thomas, and D. W. Burgess, 1998: The National Severe Storms Laboratory mesocyclone detection algorithm for the WSR-88D. *Wea. Forecasting*, **13**, 304-326.

Thompson, R. L., R. Edwards, J.A. Hart, K.L. Elmore and P.M. Markowski, 2003: Close proximity soundings within supercell environments obtained from the Rapid Update Cycle. *Wea. Forecasting*, **18**, 1243-1261.

Thompson, R. L., J. S. Grams, and J. A. Prentice, 2008: Synoptic environments and convective modes associated with significant tornadoes in the contiguous United States. Preprints, *24th Conf. Severe Local Storms*, Savannah, GA, Amer. Meteor. Soc., 16A.3.

_____, B. T. Smith, J. S. Grams, A. R. Dean, and C. Broyles, 2010: Climatology of near-storm environments with convective modes for significant severe thunderstorms in the contiguous United States. Preprints, *25th Conf. Severe Local Storms*, Denver, CO, Amer. Meteor. Soc., 16B.6.

Trapp, R. J. and M. L. Weisman, 2003: Low-Level Mesovortices within Squall Lines and Bow Echoes. Part II: Their Genesis and Implications. *Mon. Wea. Rev.*, **131**, 2804-2823.

_____, S. A. Tessendorf, E. S. Godfrey, and H. E. Brooks, 2005: Tornadoes from squall lines and bow echoes. Part I: climatological distribution. *Wea. Forecasting*, **20**, 23-34.

_____, D. M. Wheatley, N. T. Atkins, R. W. Przybylinski, and R. Wolf, 2006: Buyer beware: Some words of caution on the use of severe wind reports in postevent assessment and research. *Wea. Forecasting*, **21**, 408-415.

Weisman, M. L. and R. J. Trapp, 2003: Low-level mesovortices within squall lines and bow echoes. Part 1: Overview and dependence on environmental shear. *Mon. Wea. Rev.*, **131**, 2779-2803.

Weiss, S. J., J.A. Hart and P.R. Janish, 2002: An examination of severe thunderstorm wind report climatology: 1970-1999. Preprints, *21st Conf. Severe Local Storms*, San Antonio, TX, Amer. Meteor. Soc., 446-449.

Table 1. Tornado, sighail and sigwind event counts (relative frequency in parentheses) by convective mode category. Relative frequencies are color-coded in the following manner: < 0.100 (light gray), 0.100-0.249 (black), 0.250 - 0.499 (bold black), and ≥ 0.500 (bold red).

Mode	**tornado**		**sighail**		**sigwind**	
Total events	8176		3361		5500	
Any mode	8149	(1.000)	3336	(1.000)	5488	(1.000)
Discrete RM	2496	(**0.306**)	1622	(**0.486**)	472	(0.086)
Cluster RM	2400	(**0.295**)	993	(**0.298**)	800	(0.146)
Line RM	951	(0.117)	172	(0.052)	351	(0.064)
Discrete LM	19	(0.002)	235	(0.070)	53	(0.010)
Cluster LM	10	(0.001)	152	(0.046)	42	(0.008)
Line LM	0	(0.000)	9	(0.003)	3	(0.001)
Discrete or cluster RM + LM	4925	(**0.604**)	2613	(**0.783**)	1367	(0.249)
All RM	5847	(**0.718**)	2787	(**0.835**)	1623	(**0.296**)
All LM	29	(0.004)	396	(0.119)	98	(0.018)
All RM + LM	5876	(**0.721**)	3183	(**0.954**)	1721	(**0.314**)
Linear hybrid (subset line RM + QLCS)	231	(0.028)	3	(0.001)	146	(0.027)
Bow Echo (subset QLCS)	137	(0.017)	5	(0.001)	503	(0.092)
QLCS	987	(0.121)	27	(0.008)	1983	(**0.361**)
Any line (QLCS + line RM or LM)	1938	(0.238)	208	(0.062)	2337	(**0.426**)
Marginal supercell	288	(0.035)	51	(0.015)	117	(0.021)
Disorganized	998	(0.122)	75	(0.022)	1668	(**0.304**)
No data	27	(0.003)	25	(0.007)	11	(0.002)

Table 2. Tornado event count (relative frequency in parentheses) by F-scale damage for each convective mode category. Other conventions are the same as Table 1.

Mode	**F0+**	**F1+**	**F2+**	**F3+**	**F4+**
Total events	8176	3315	977	259	39
Any mode	8149 (1.000)	3304 (1.000)	976 (1.000)	259 (1.000)	39 (1.000)
Discrete RM	2496 (**0.306**)	1046 (**0.317**)	418 (**0.428**)	135 (**0.521**)	24 (**0.615**)
Cluster RM	2400 (**0.295**)	1035 (**0.313**)	303 (**0.310**)	81 (**0.313**)	12 (**0.308**)
Line RM	951 (0.117)	556 (0.168)	166 (0.170)	37 (0.143)	3 (0.077)
Discrete LM	19 (0.002)	3 (0.001)	0 (0.000)	0 (0.000)	0 (0.000)
Cluster LM	10 (0.001)	4 (0.001)	0 (0.000)	0 (0.000)	0 (0.000)
Line LM	0 (0.000)	0 (0.000)	0 (0.000)	0 (0.000)	0 (0.000)
Discrete or cluster RM + LM	4925 (**0.604**)	2088 (**0.632**)	721 (**0.739**)	216 (**0.834**)	36 (**0.923**)
All RM	5847 (**0.718**)	2637 (**0.798**)	887 (**0.909**)	253 (**0.977**)	39 (**1.000**)
All LM	29 (0.004)	7 (0.002)	0 (0.000)	0 (0.000)	0 (0.000)
All RM + LM	5876 (**0.721**)	2644 (**0.800**)	887 (**0.909**)	253 (**0.977**)	39 (**1.000**)
Linear hybrid (subset line RM + QLCS)	231 (0.028)	147 (0.044)	34 (0.035)	8 (0.031)	1 (0.026)
Bow Echo (subset QLCS)	137 (0.017)	86 (0.026)	25 (0.026)	5 (0.020)	0 (0.000)
QLCS	987 (0.121)	490 (0.148)	76 (0.078)	5 (0.020)	0 (0.000)
Any line (QLCS + line RM)	1938 (0.238)	1046 (**0.317**)	242 (0.248)	42 (0.162)	3 (0.077)
Marginal supercell	288 (0.035)	55 (0.017)	7 (0.007)	0 (0.000)	0 (0.000)
Disorganized	998 (0.122)	115 (0.035)	6 (0.006)	1 (0.004)	0 (0.000)
No data	27 (0.003)	11 (0.003)	1 (0.001)	0 (0.000)	0 (0.000)

Table 3. Mesocyclone strength by tornado F-scale damage for all RM. Other conventions the same as Table 1.

RM	**F0 (3210)**	**F1 (1750)**	**F2 (634)**	**F3 (214)**	**F4+ (39)**
Weak	1468 (**0.457**)	536 (**0.306**)	69 (0.109)	7 (0.033)	0 (0.000)
Moderate	873 (**0.272**)	502 (**0.287**)	117 (0.185)	19 (0.089)	1 (0.026)
Strong	869 (**0.271**)	712 (**0.407**)	448 (**0.707**)	188 (**0.879**)	38 (**0.974**)

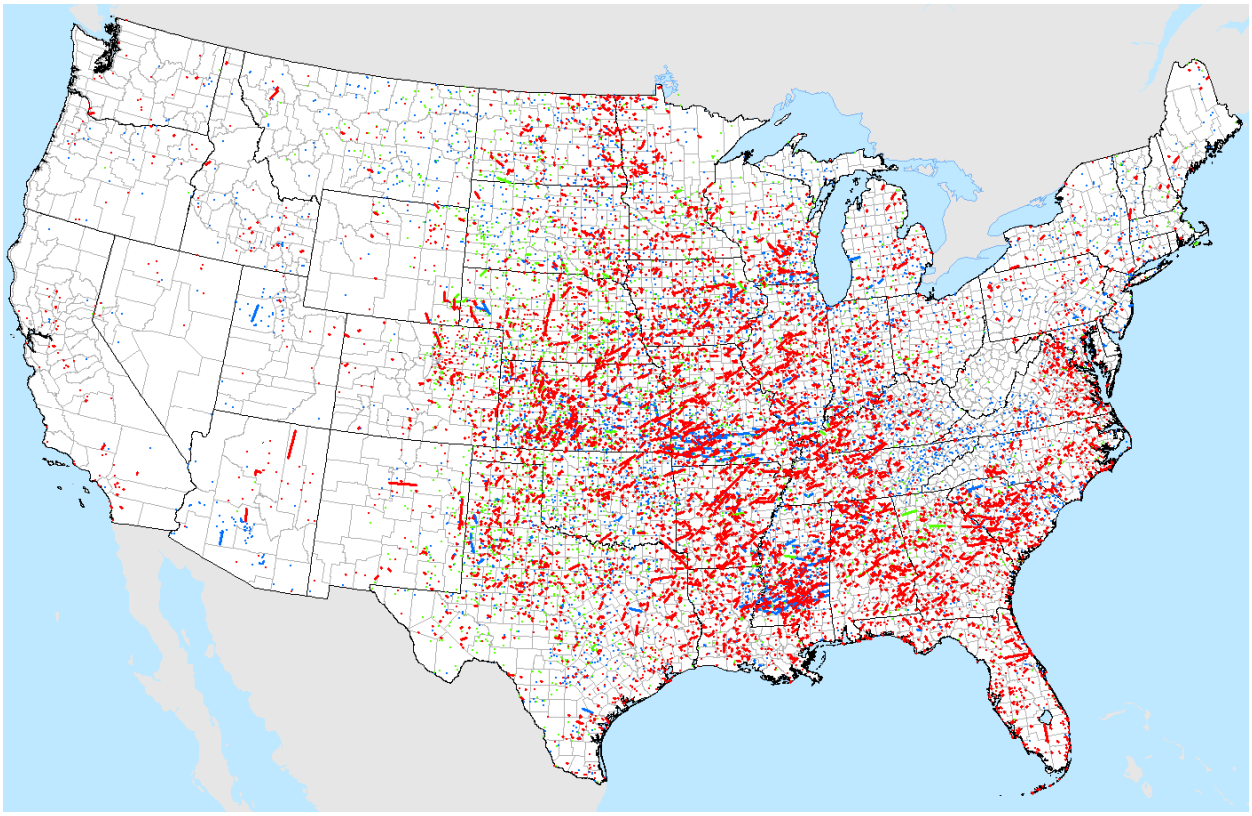

Figure 1. All tornado (red), sighail (green), and sigwind (blue) events filtered for the largest magnitude event of each type on an hourly 40 km grid for the period 2003-2009.

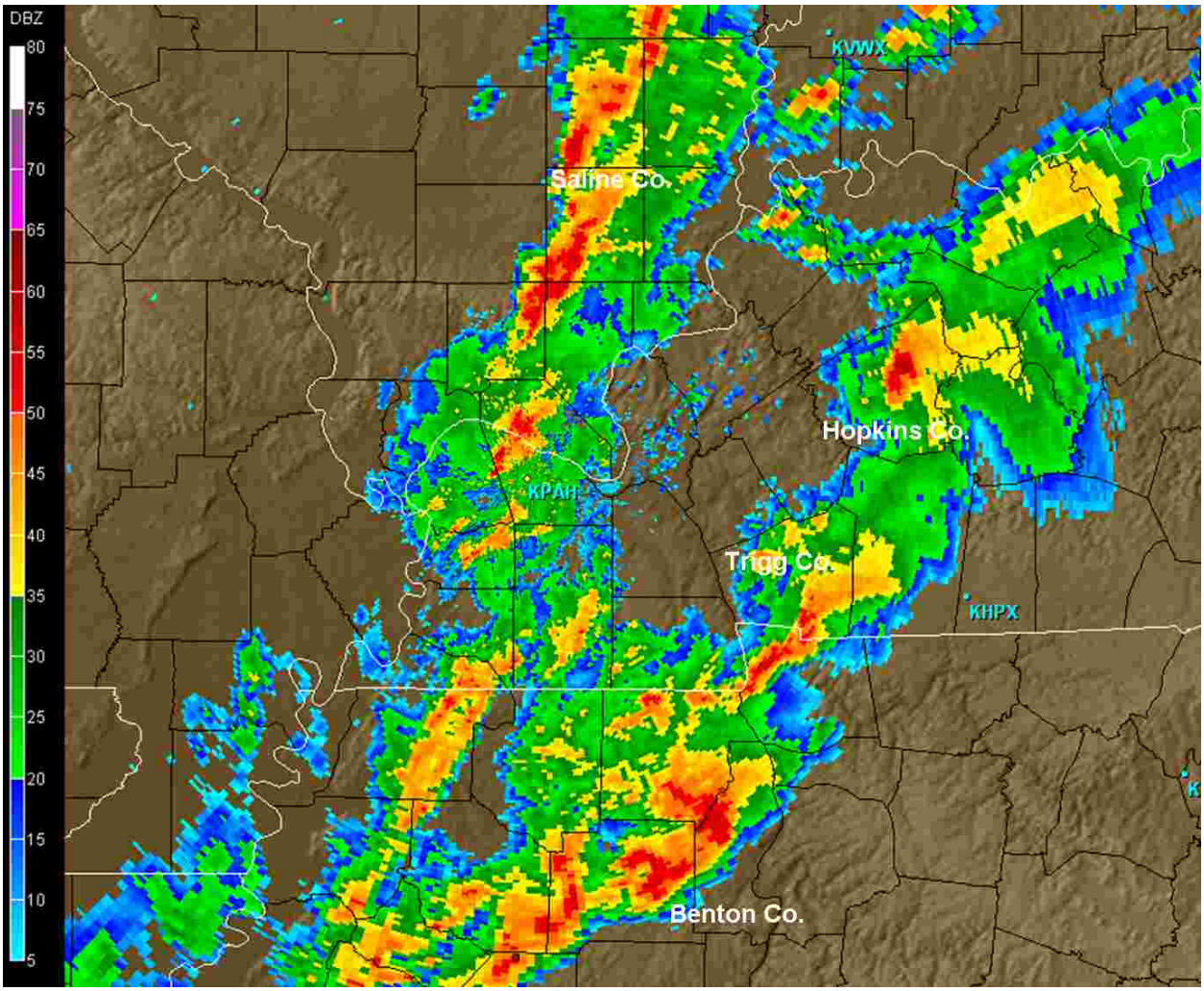

Figure 2. WSR-88D base reflectivity (dBZ, color scale on left) at 0.5º beam tilt from Paducah, KY (KPAH) at 2132 UTC on 15 November 2005. A discrete RM produced an F4 tornado in Hopkins County KY (start time 2127 UTC), and F0 tornado and sigwind report occurred with the QLCS in Saline County, IL (2132 UTC), a cluster RM in Trigg County, KY (2135 UTC), and a line RM in Benton County, TN that produced F1 and F2 tornado events at 2135 and 2138 UTC, respectively. North is up; state (county) borders are white (black); radar locations labeled cyan.

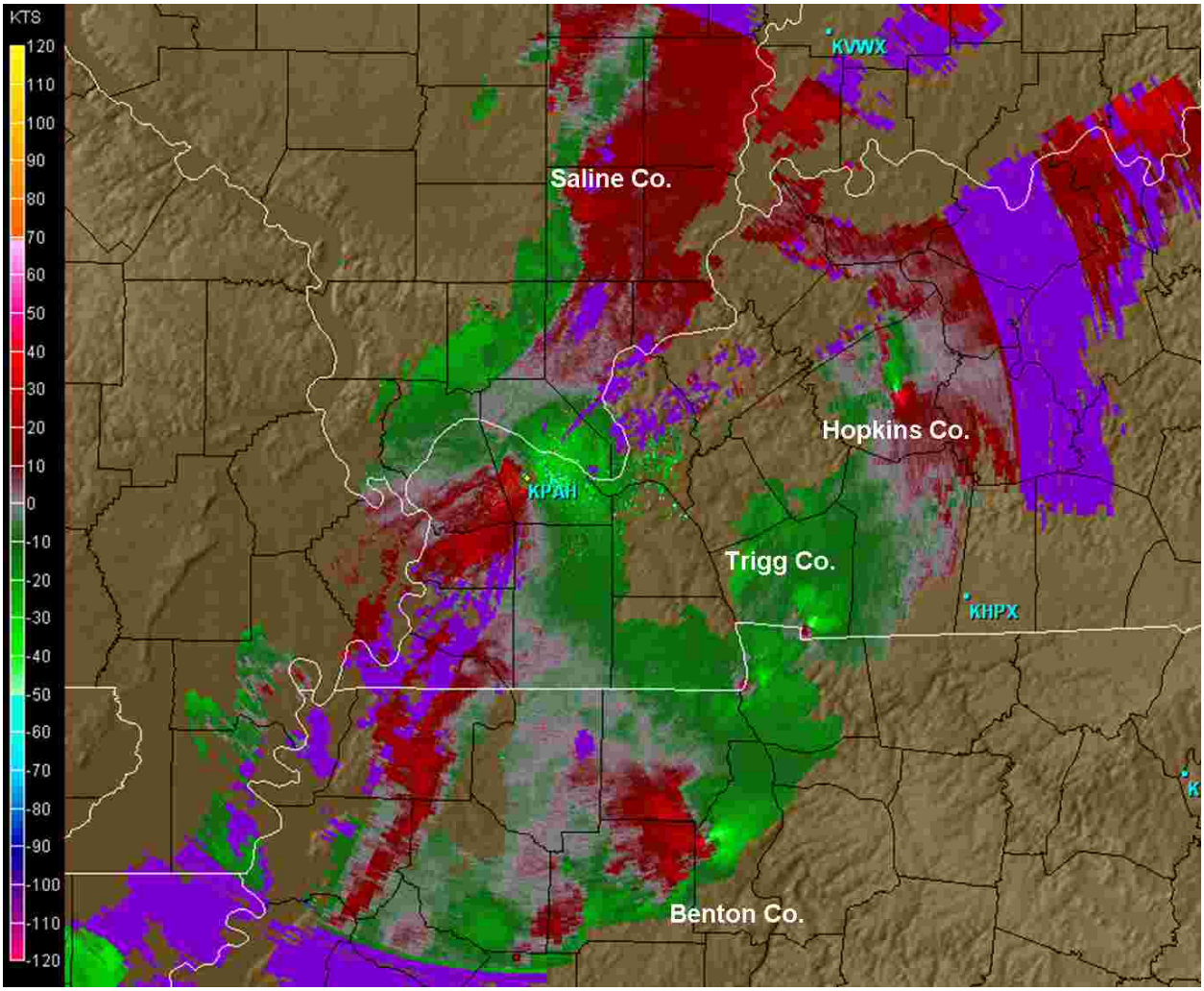

Figure 3. Same as Fig. 2, except for storm relative velocity (kt, scale on left).

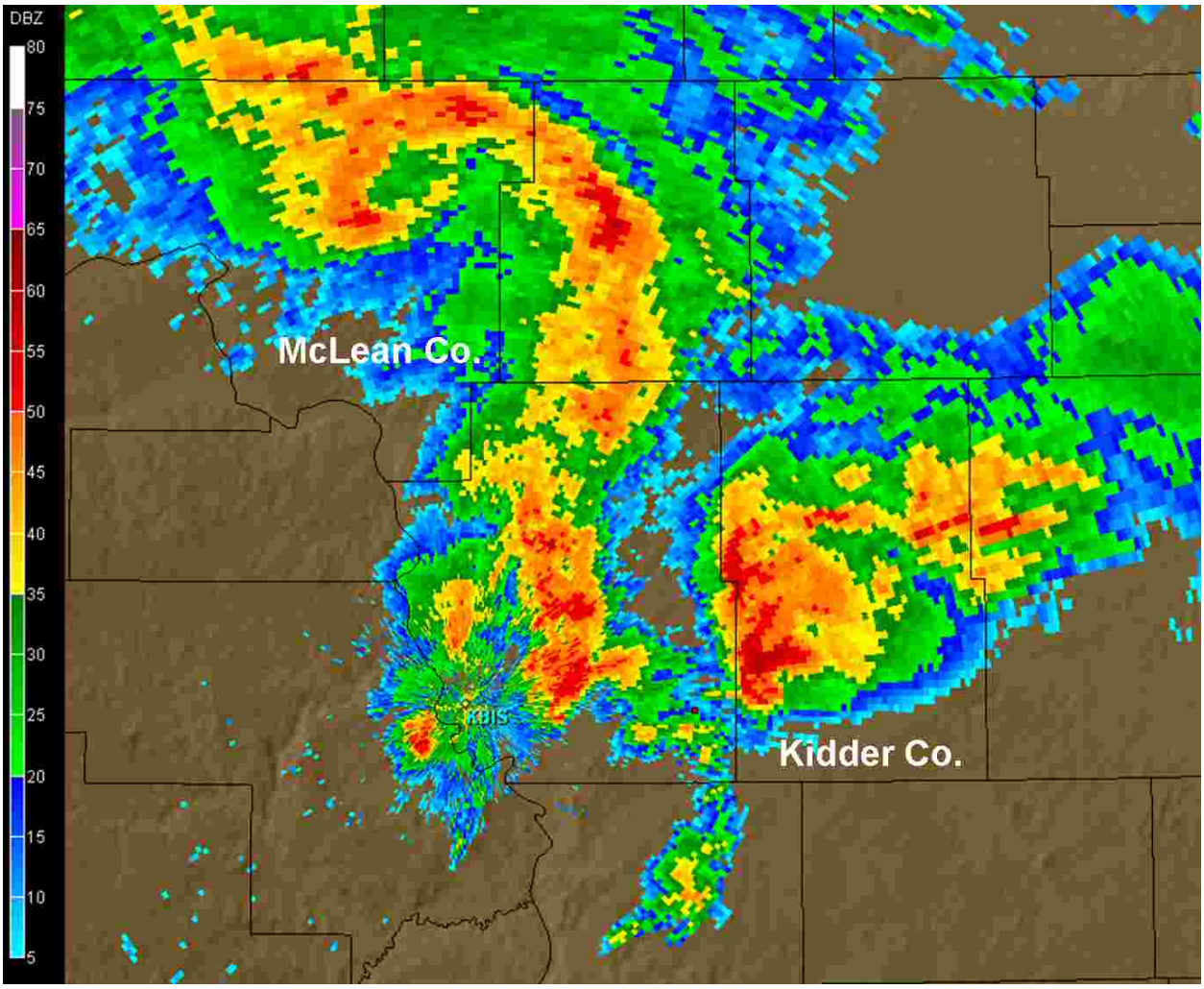

Figure 4. Same as Fig. 2, except for Bismarck, ND (KBIS) at 1956 UTC on 24 August 2006. A cluster RM produced an F0 tornado in Kidder County ND (report start time 2003 UTC). The bow echo in McLean County, ND was responsible for an F2 tornado event (1855 UTC) and two sigwind events (1920 UTC, 1945 UTC). Same label conventions as Fig. 2.

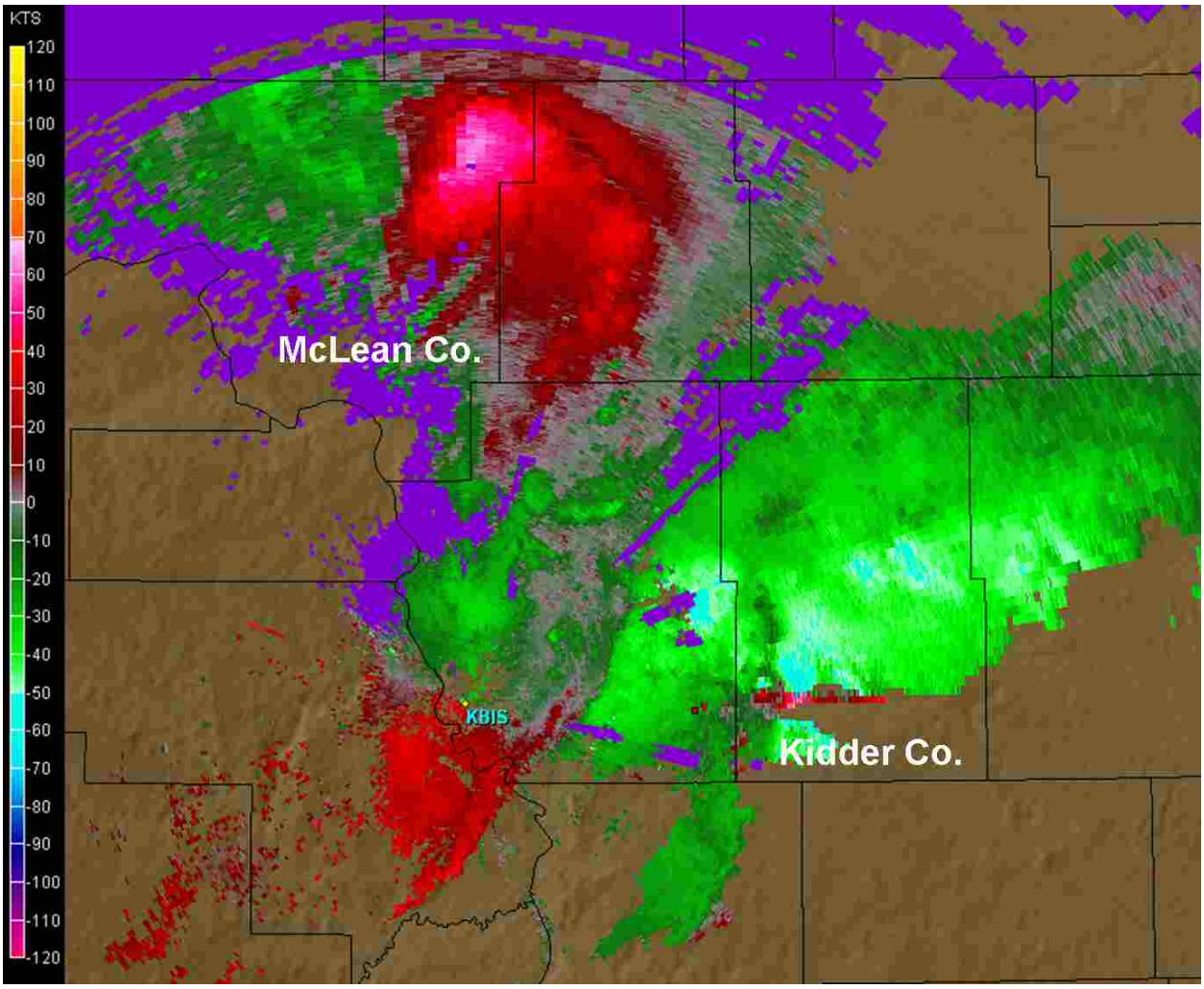

Figure 5. Same as Fig. 4, except for storm relative velocity.

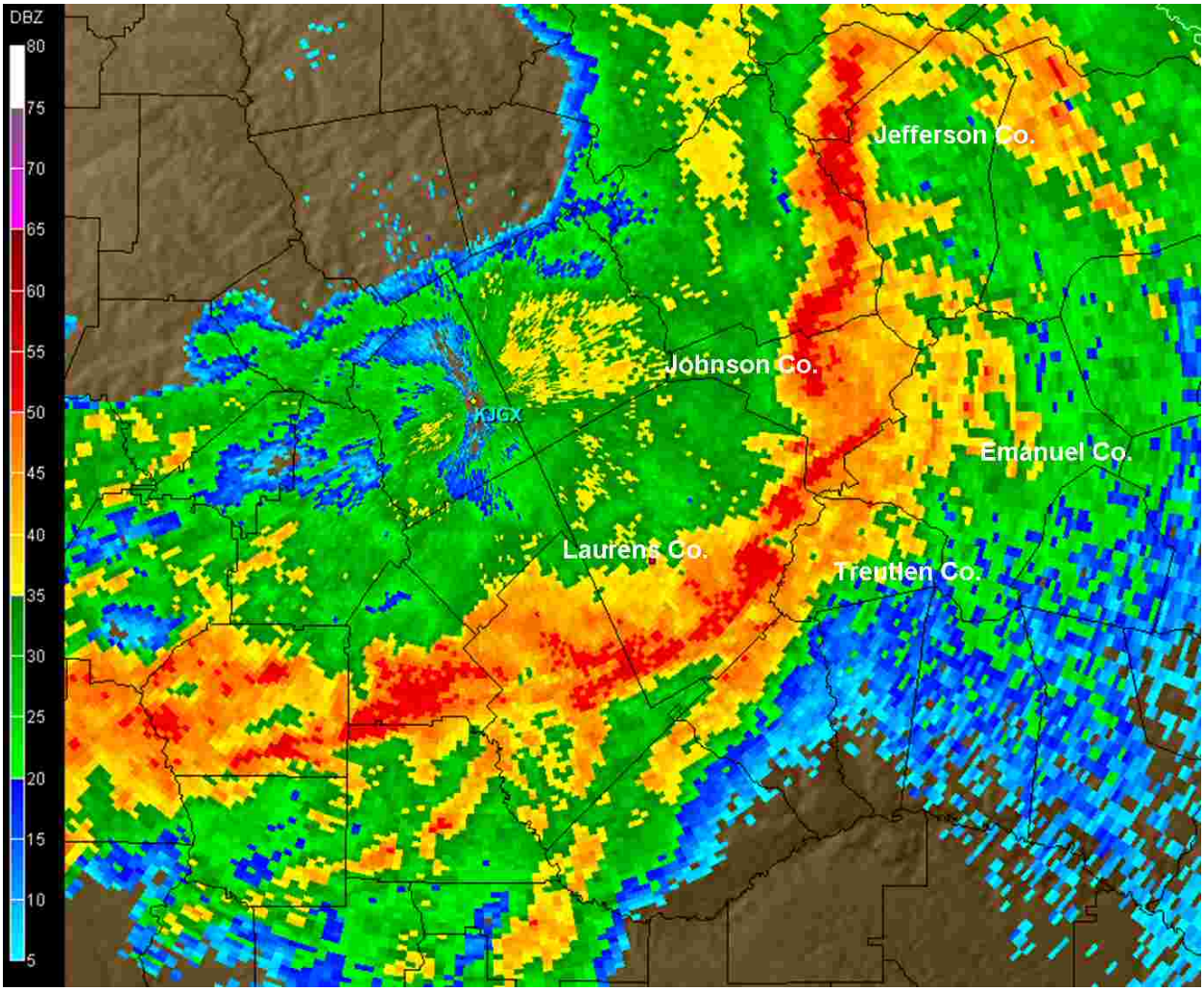

Figure 6. WSR-88D base reflectivity image (0.5º beam tilt) from Robins AFB, GA (KJGX) at 1057 UTC on 11 May 2008. A line RM produced an F0 tornado in Jefferson County, GA (report start time 1057 UTC); an F0 tornado was associated with the bow echo "mesovortex" in Laurens County (1058 UTC); a line RM produced an F2 tornado with three injuries and sigwind events in Johnson County (1101 UTC); a line RM produced an F2 tornado and sigwind events in Emanuel County (1107 UTC); an F3 tornado was produced by a bow echo "mesovortex" in Treutlen County (1111 UTC). All events described herein were considered linear hybrids. Same label conventions as Fig. 2.

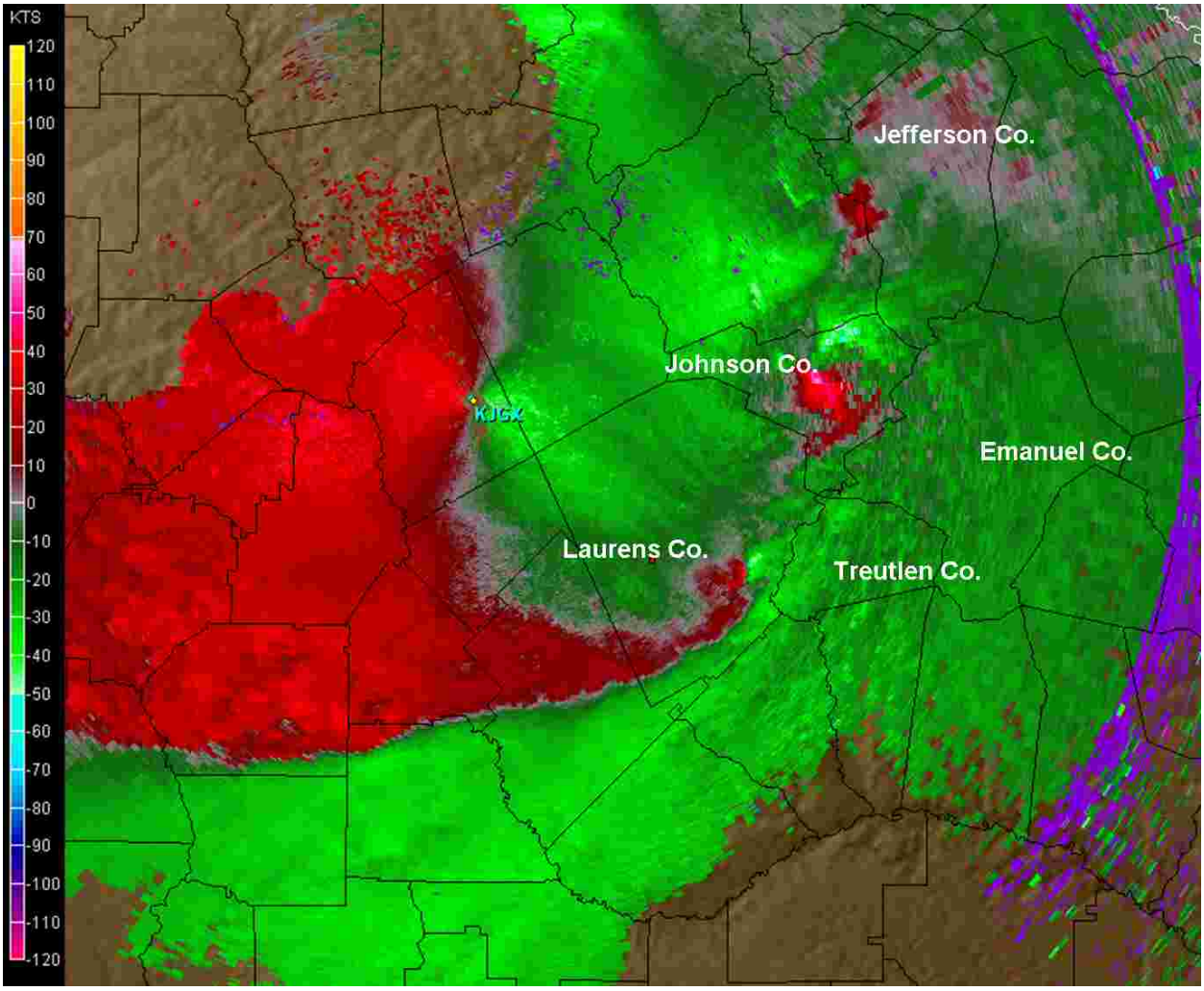

Figure 7. Same as Fig. 6, except for storm relative velocity (kt, scale on left).

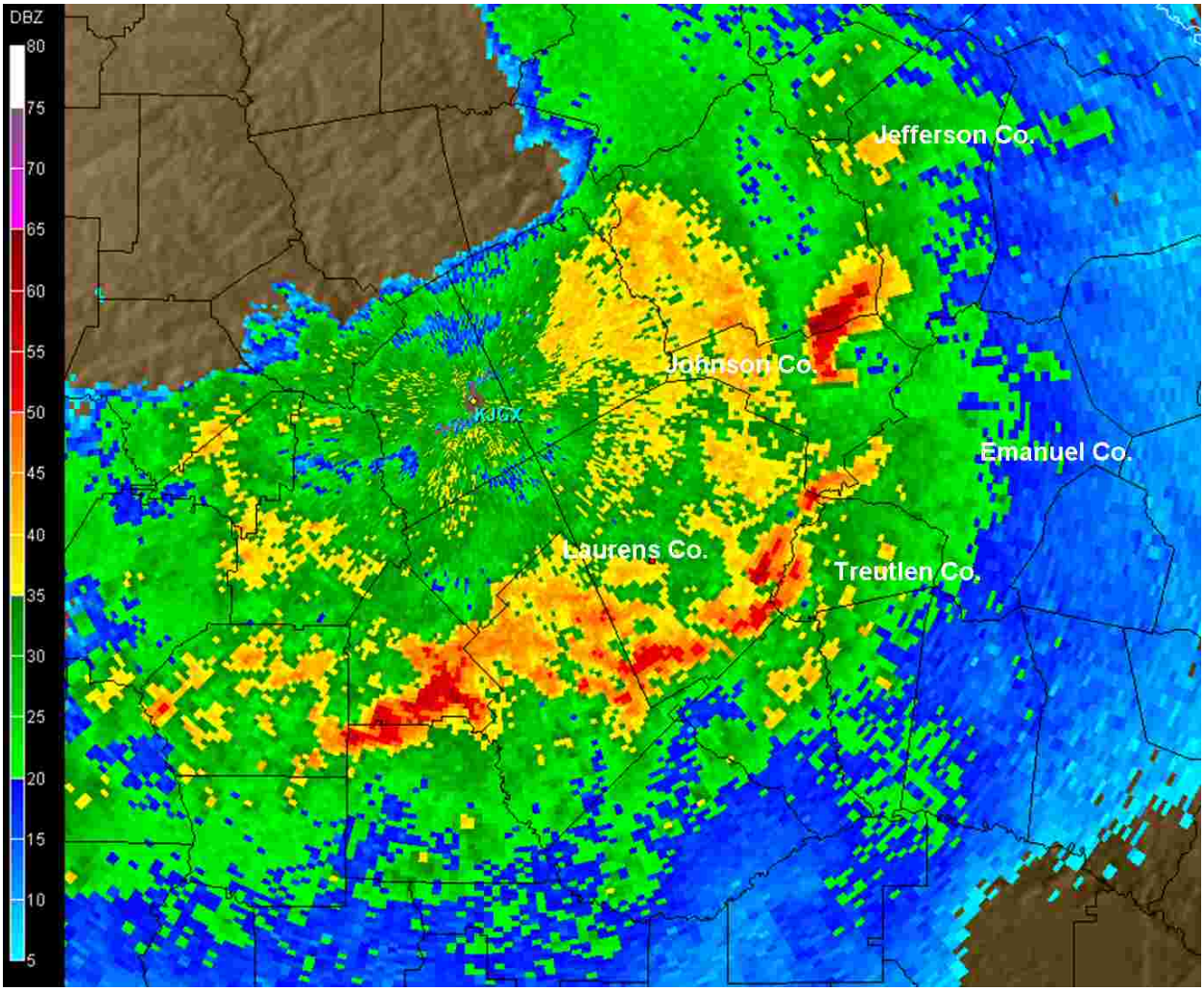

Figure 8. Same as Fig. 6, except for 3.9º beam tilt sampling Johnson County line RM near 17000 feet AGL.

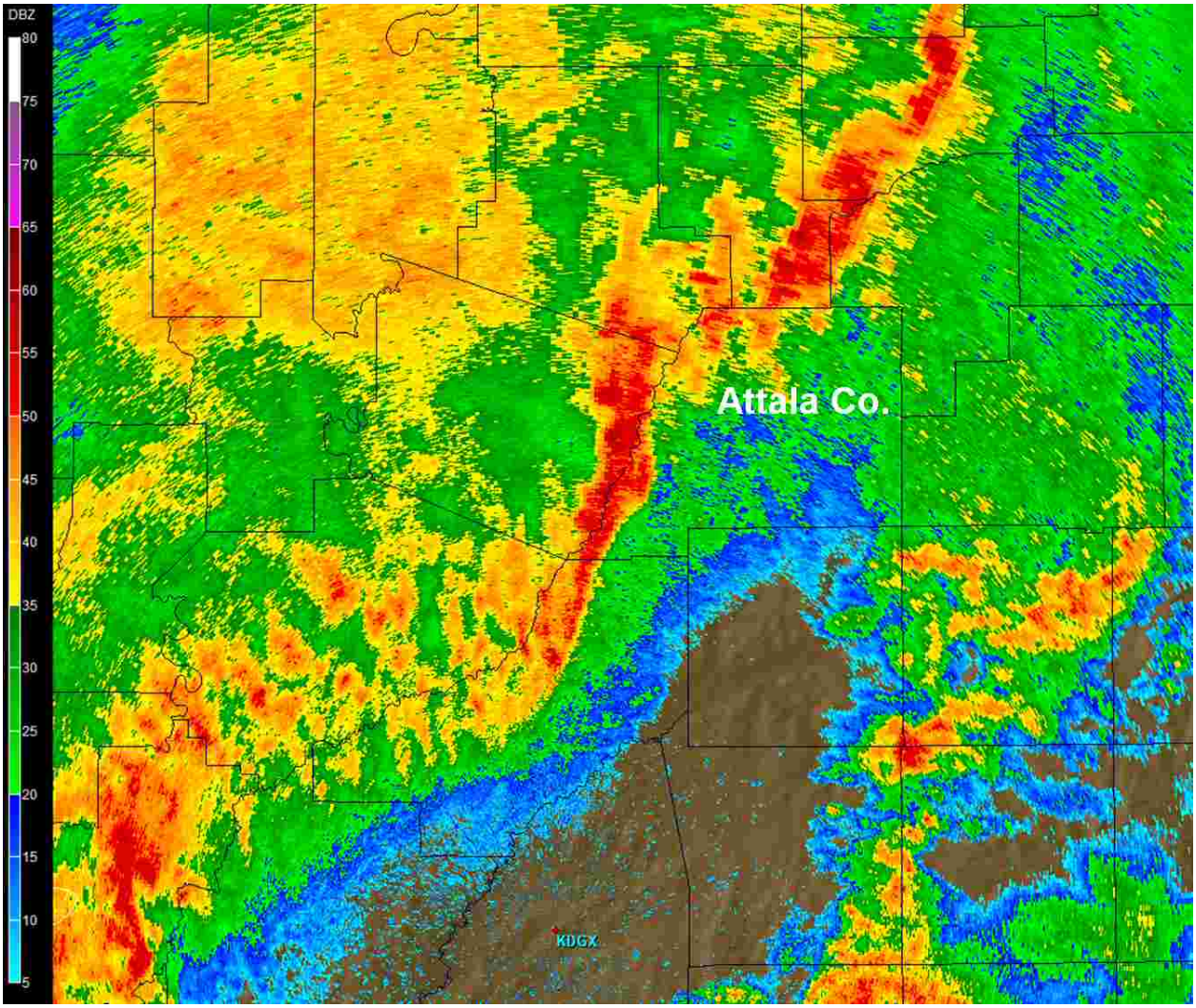

Figure 9. WSR-88D base reflectivity (0.5º beam tilt) from Jackson, MS (KDGX) at 0127 UTC on 10 December 2008. A line RM produced an F1 tornado (0127 UTC) and sigwind event (0133 UTC) in Attala County, MS. Same label conventions as Fig. 2.

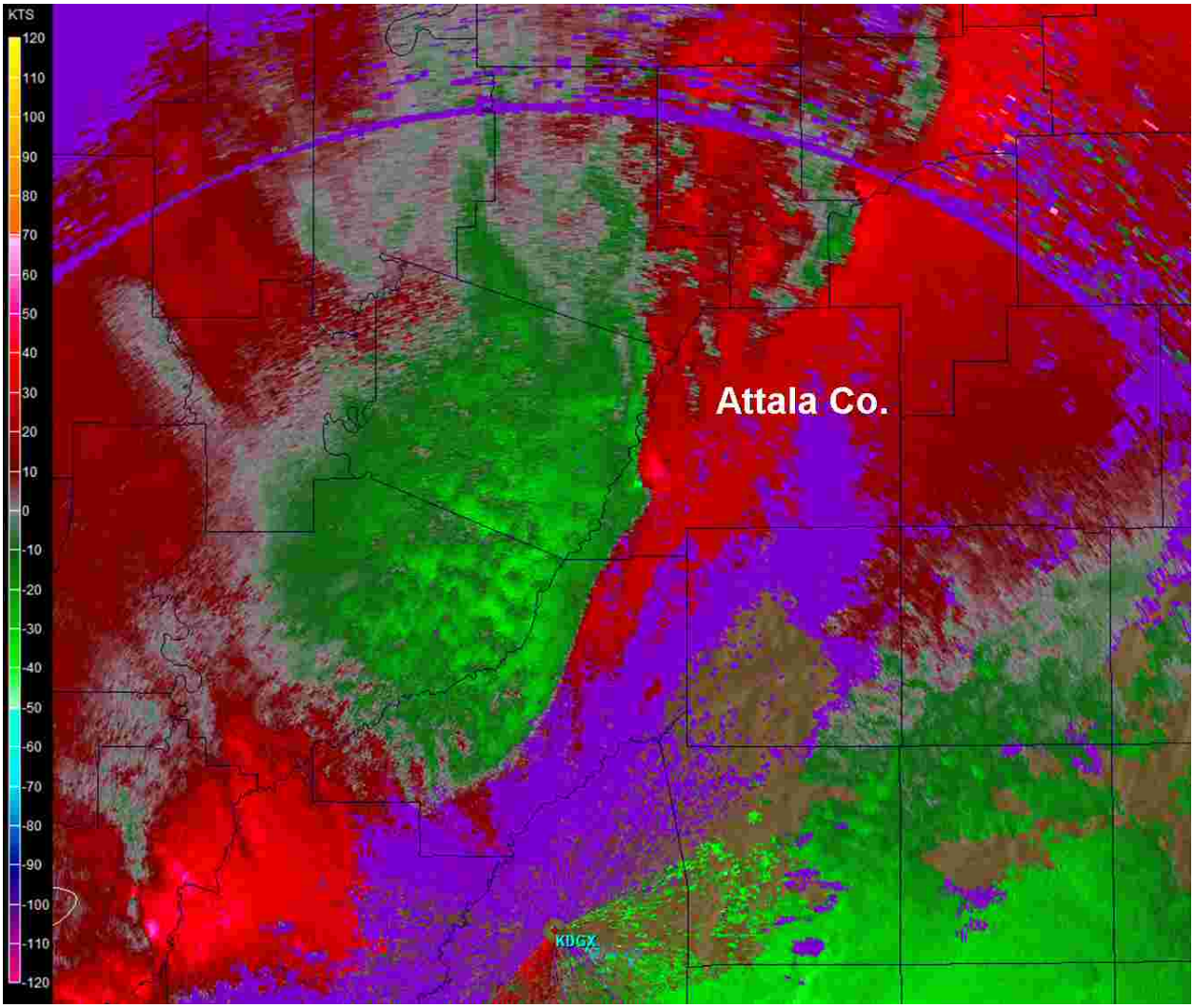

Figure 10. Same as Fig. 9, except for storm relative velocity.

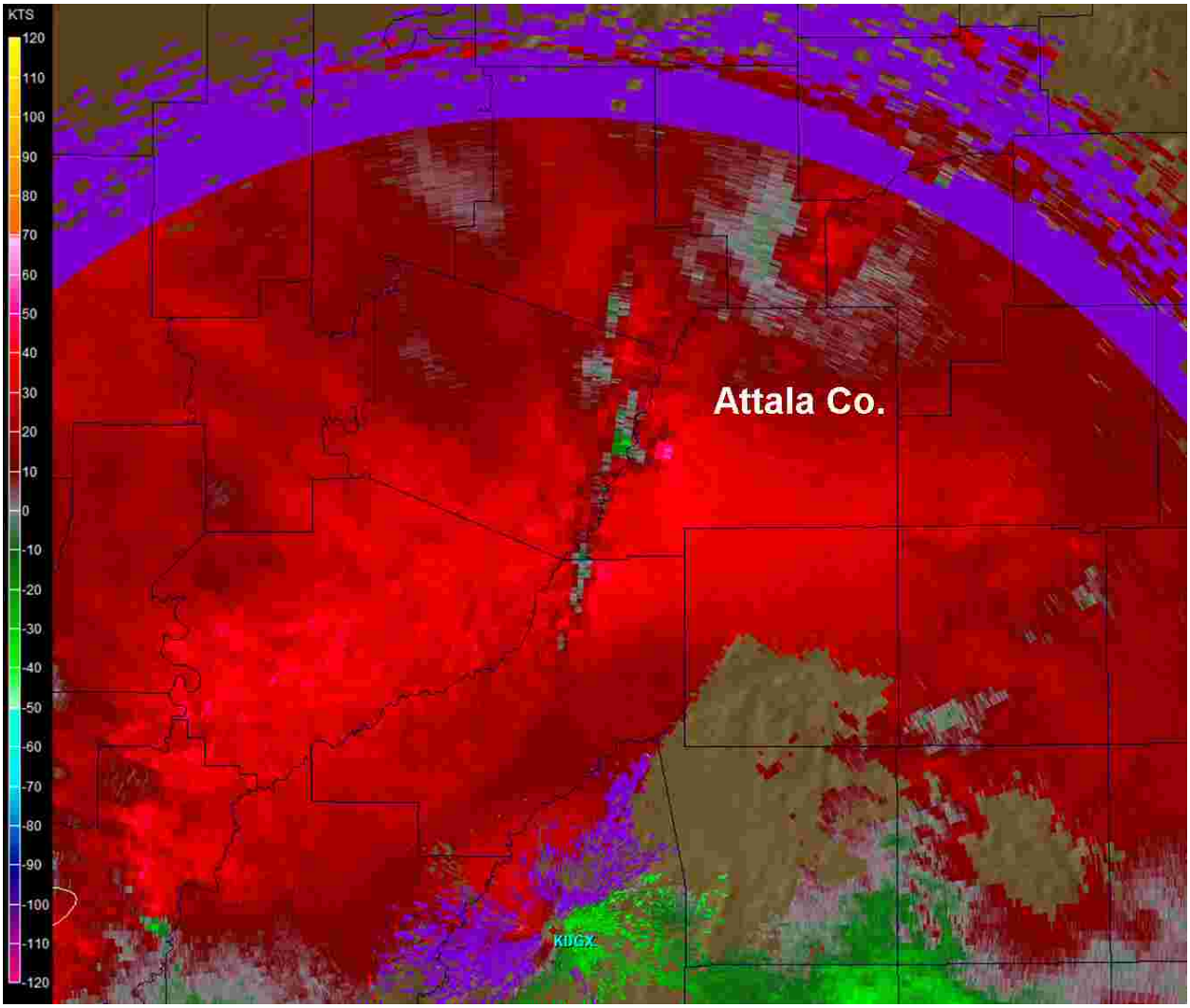

Figure 11. Same as Fig. 10, except for 3.2º beam tilt sampling Attala County line RM near 18000 feet AGL.

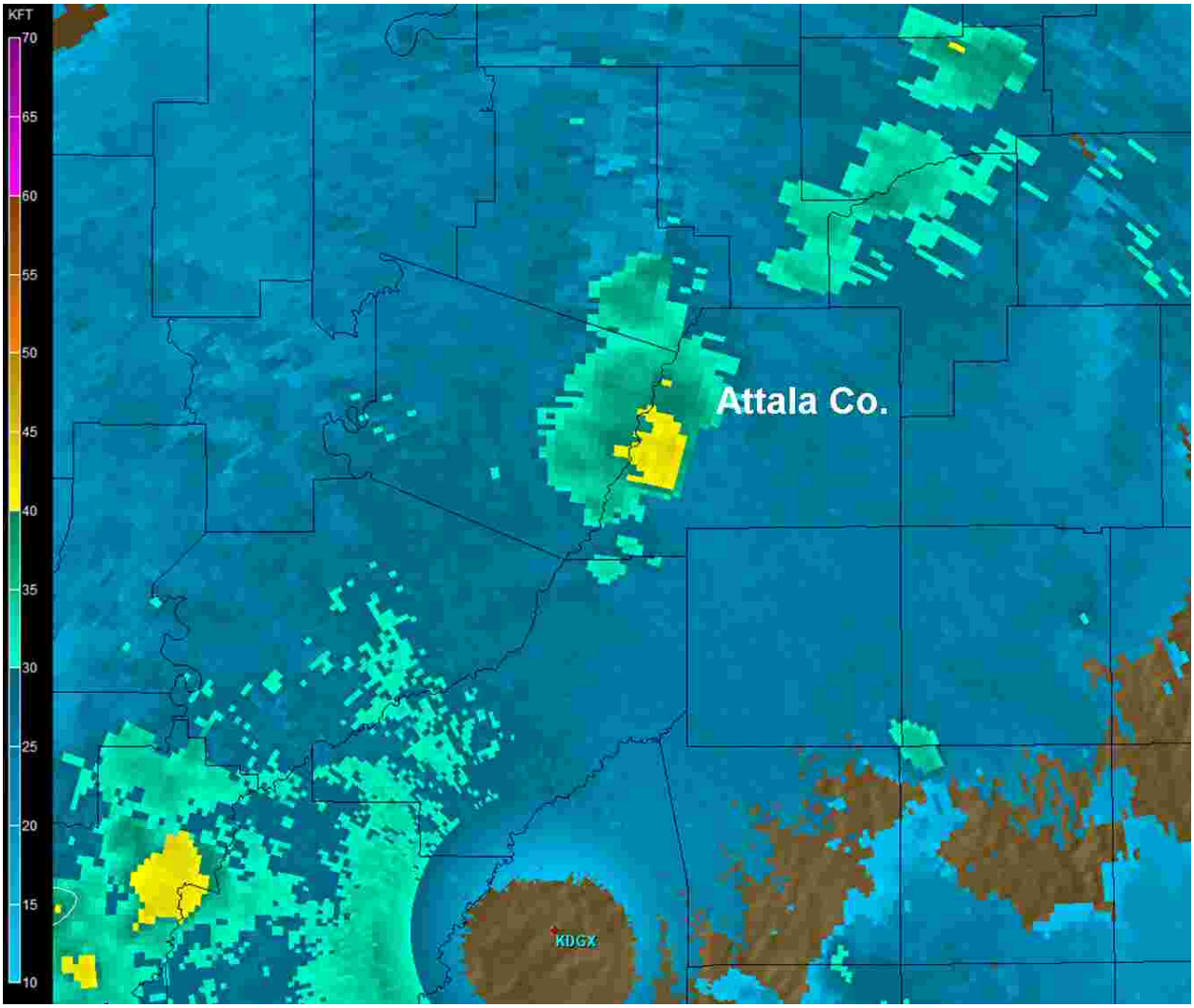

Figure 12. Same as Fig. 9, except for echo top height.

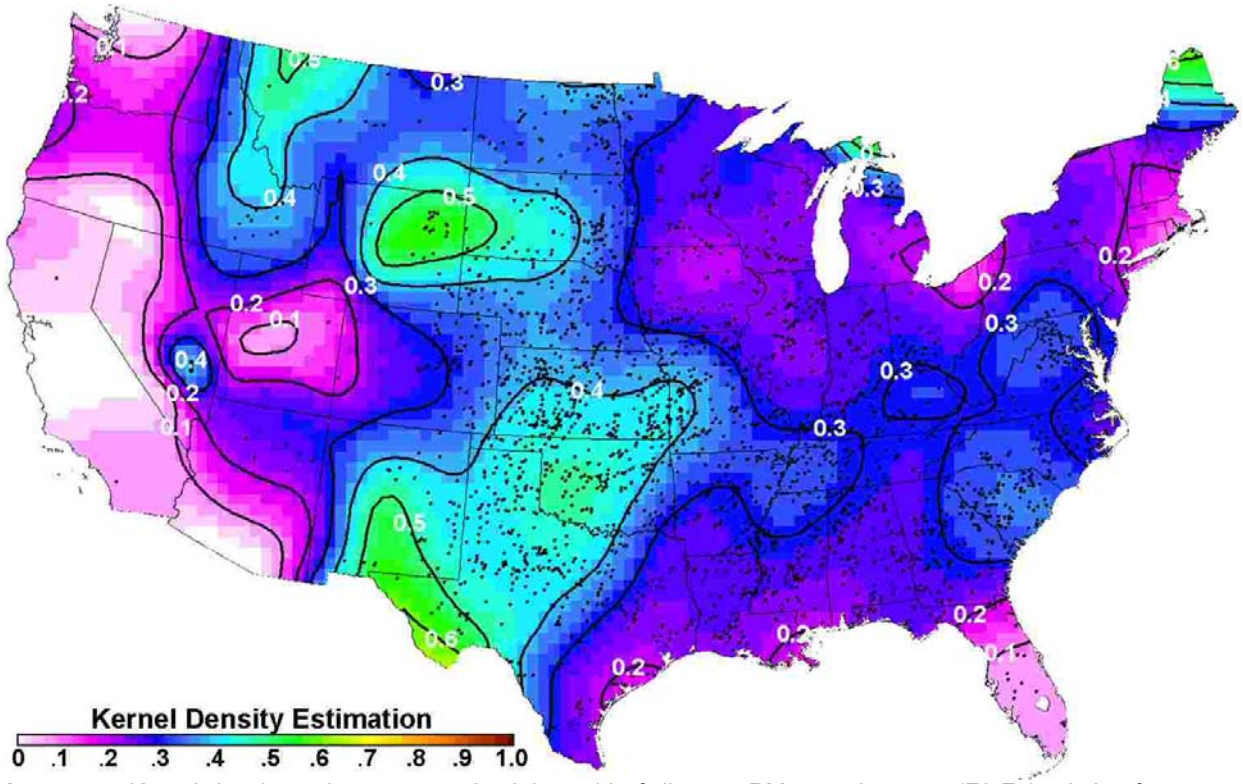

Figure 13. Kernel density estimate on a 40x40 km grid of discrete RM tornado event (F0-F5) relative frequency compared to all tornado events, with 10% contour intervals of relative frequency (black lines). Black dots represent tornado events (2496) that formed the basis of the kernel density estimate, and the color-fill legend for convective mode relative frequency is shown at the lower left.

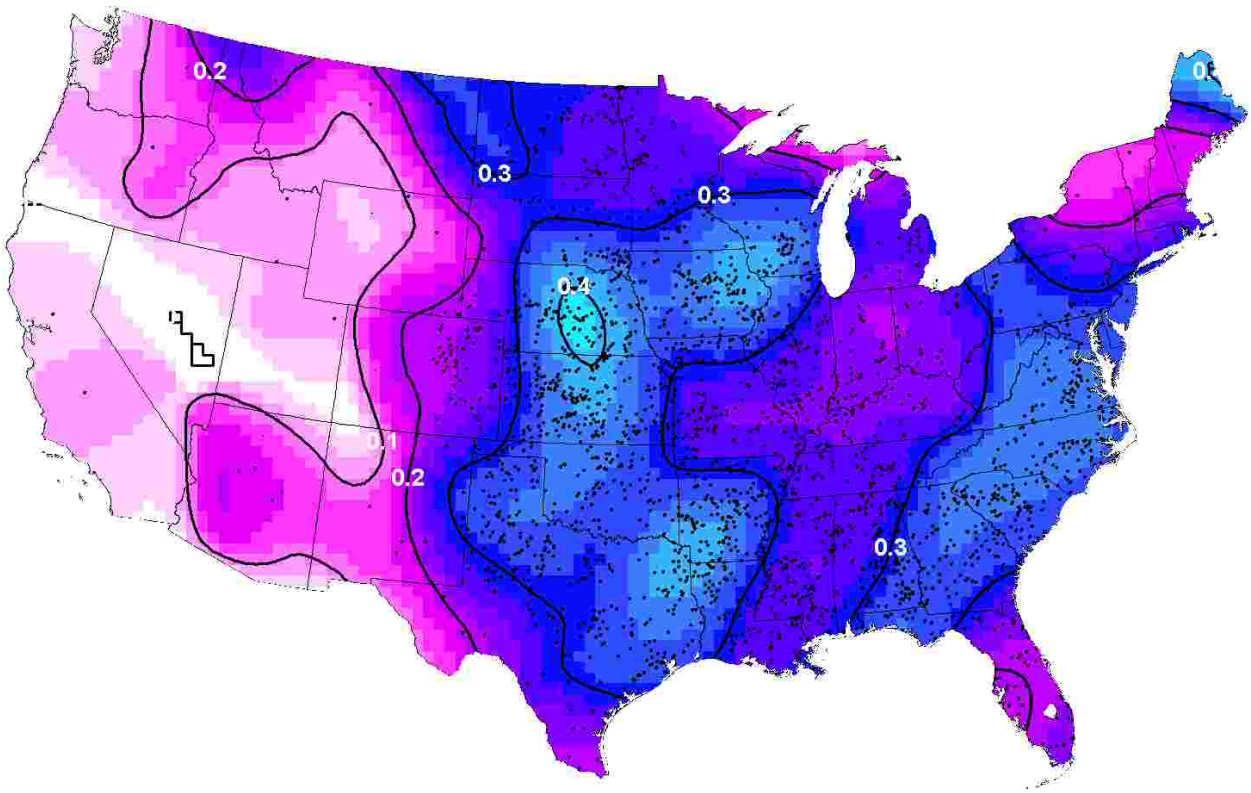

Figure 14. Same as Fig. 13 except for cluster RM (2400 events).

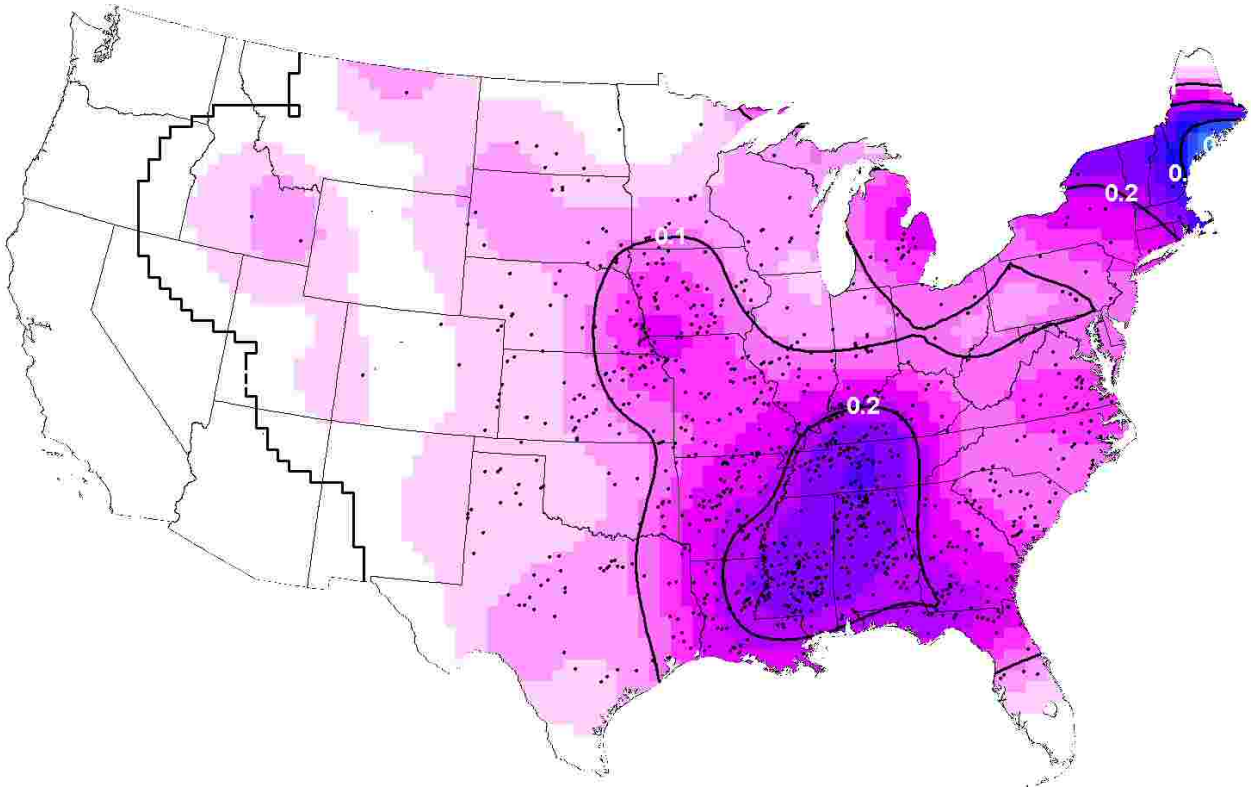

Figure 15. Same as Fig. 13 except for line RM (951 events).

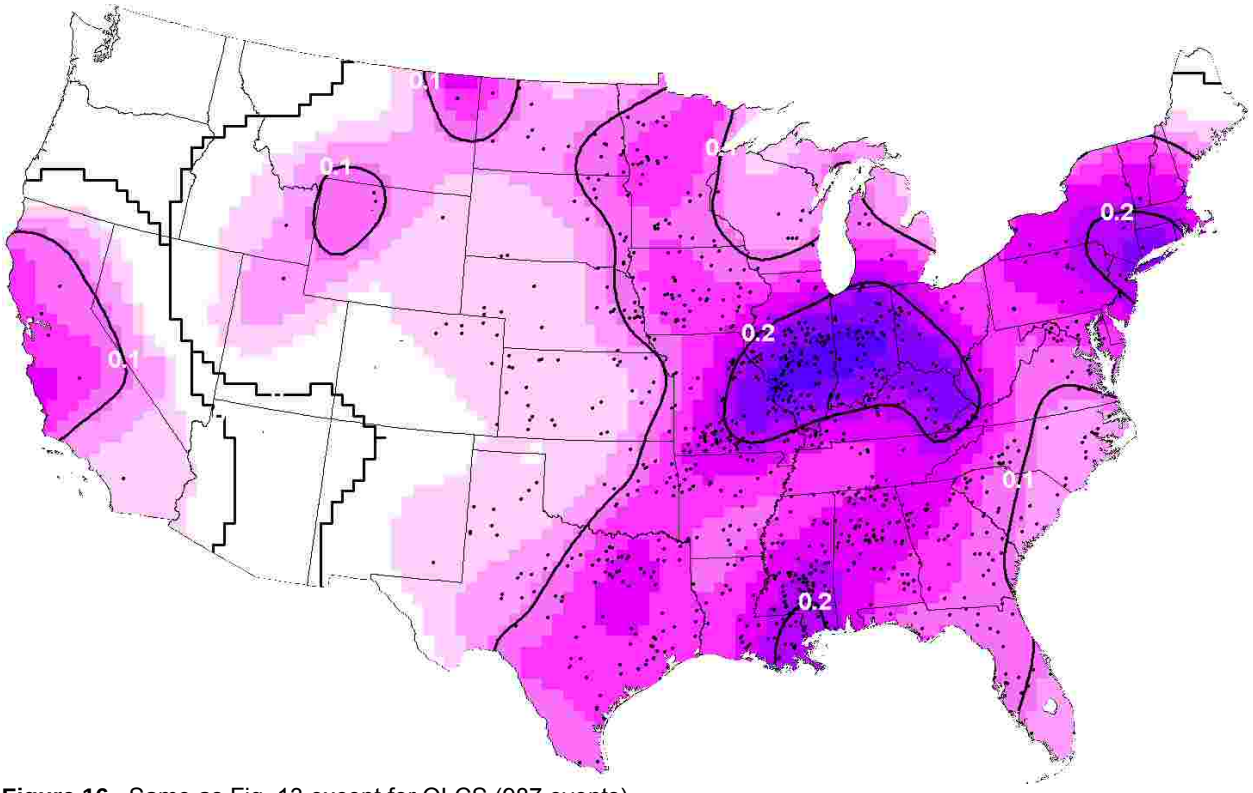

Figure 16. Same as Fig. 13 except for QLCS (987 events).

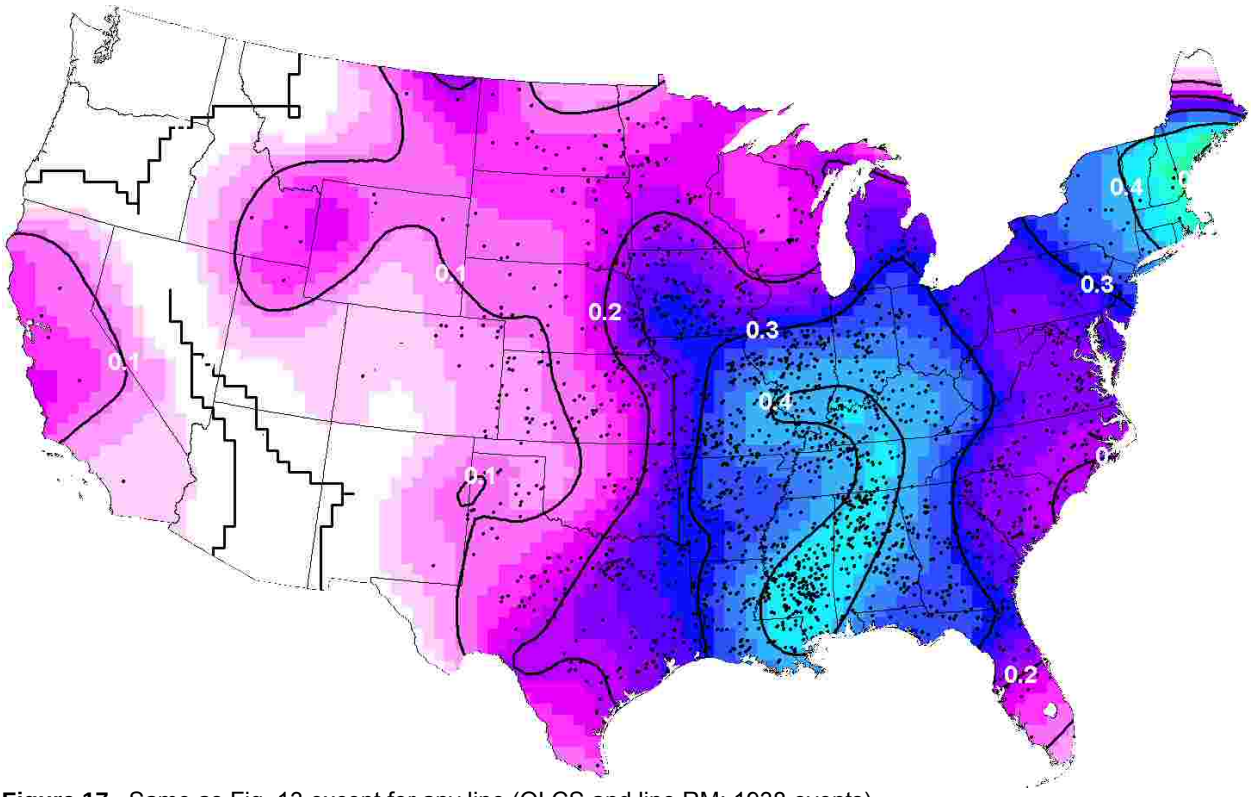

Figure 17. Same as Fig. 13 except for any line (QLCS and line RM; 1938 events).

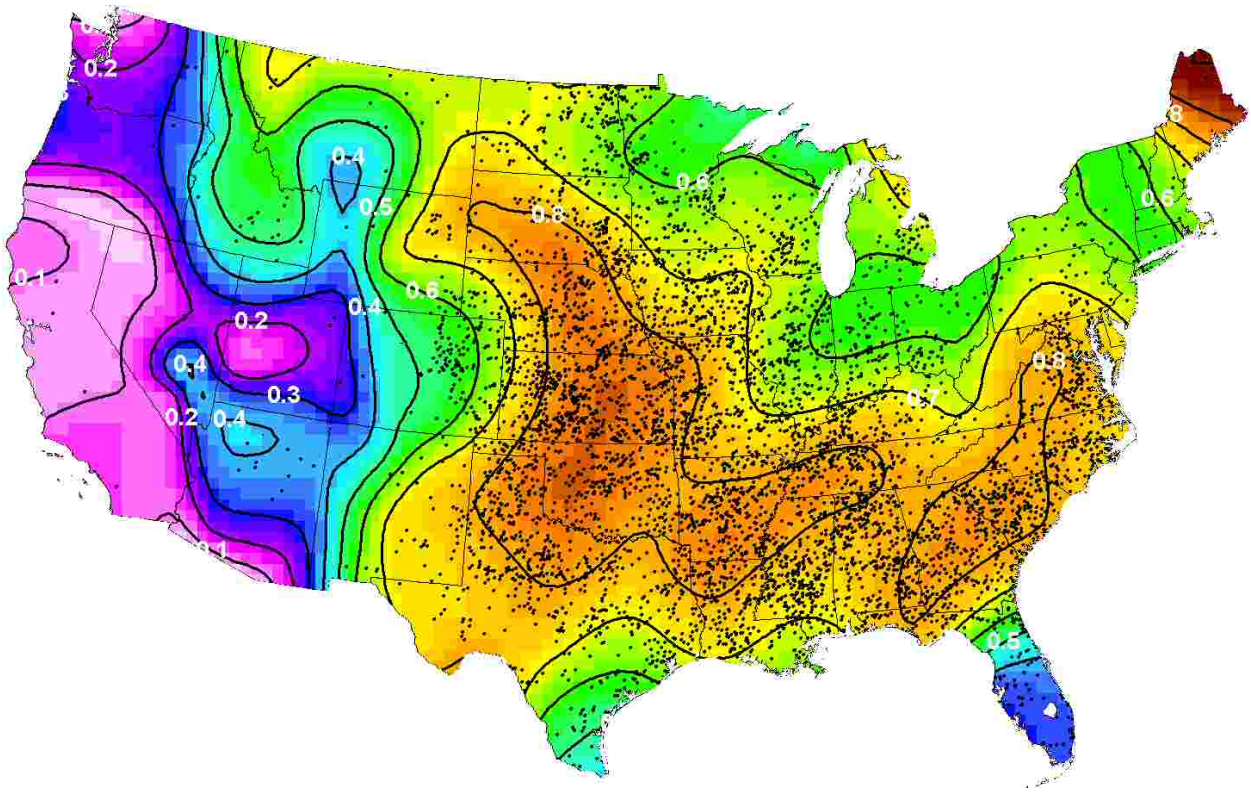

Figure 18. Same as Fig. 13 except for all RM (discrete, cluster, line; 5847 events).

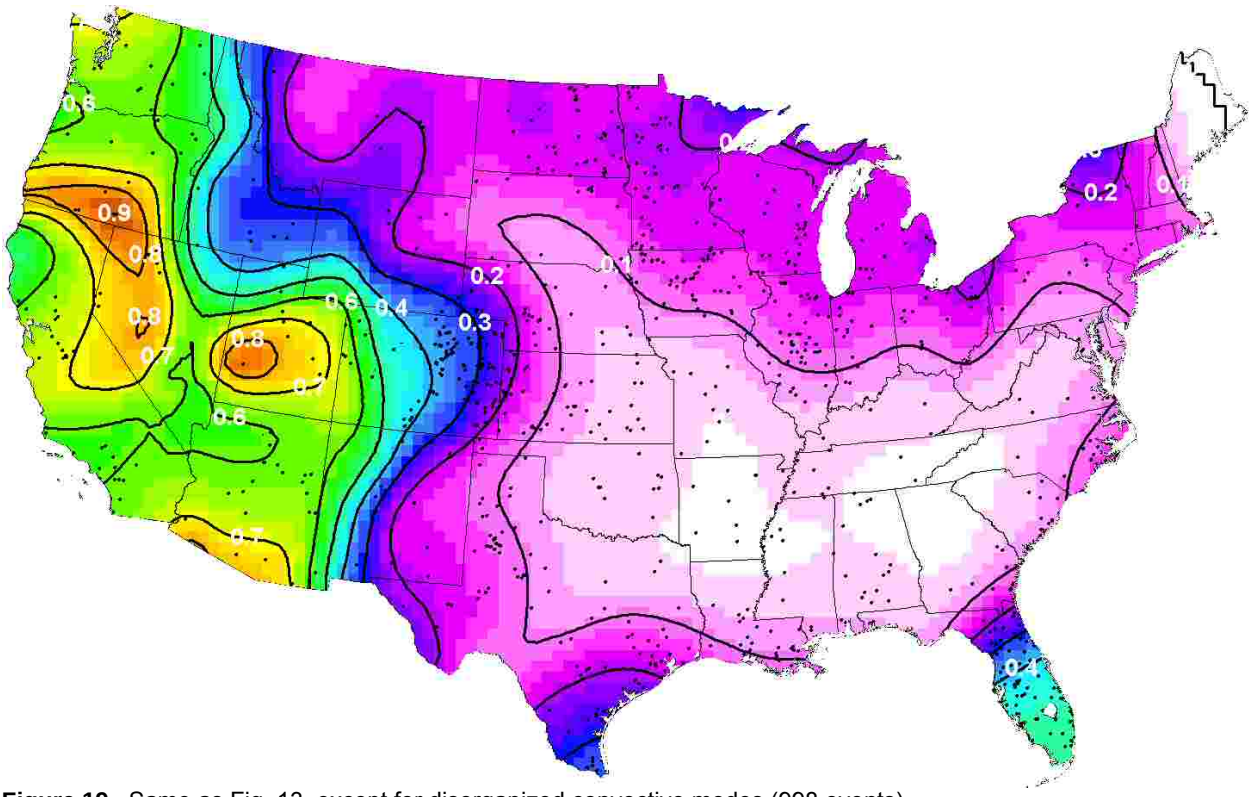

Figure 19. Same as Fig. 13, except for disorganized convective modes (998 events).

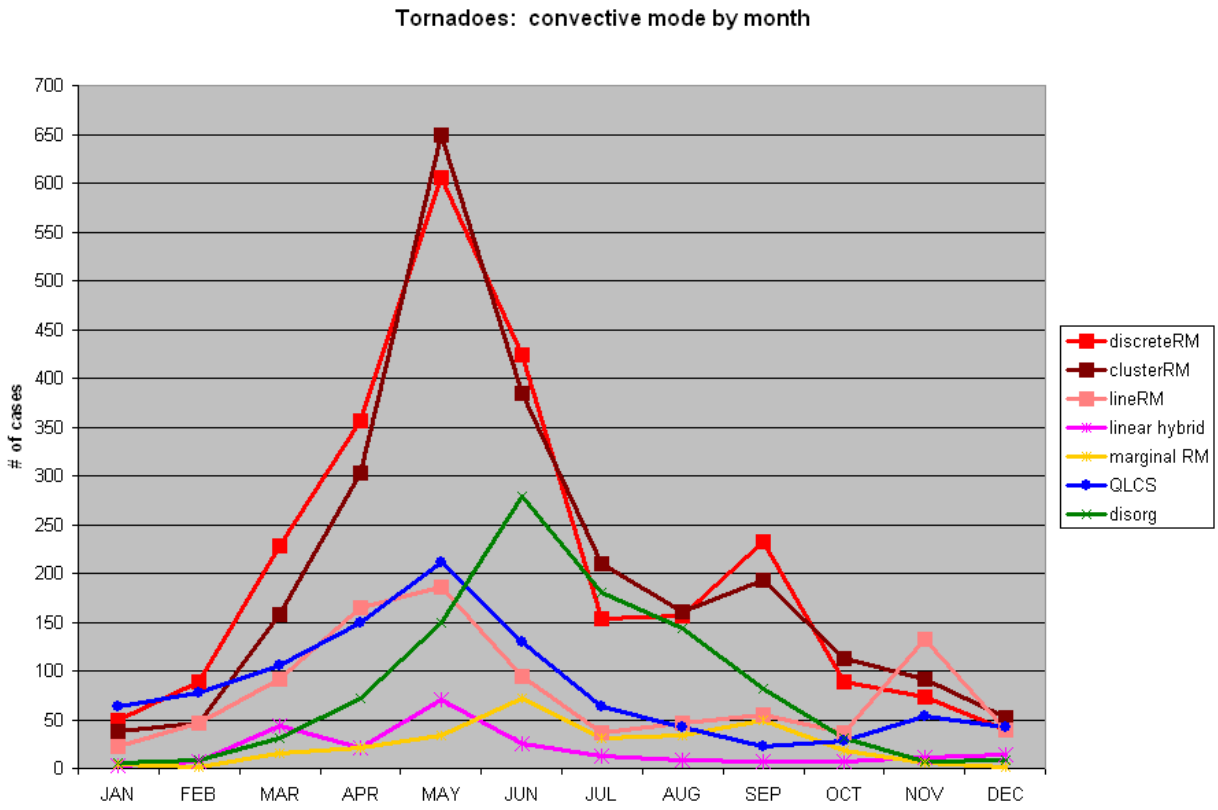

Figure 20. Tornado event convective mode count by month. Legend on right-side of image details labeling nomenclature.

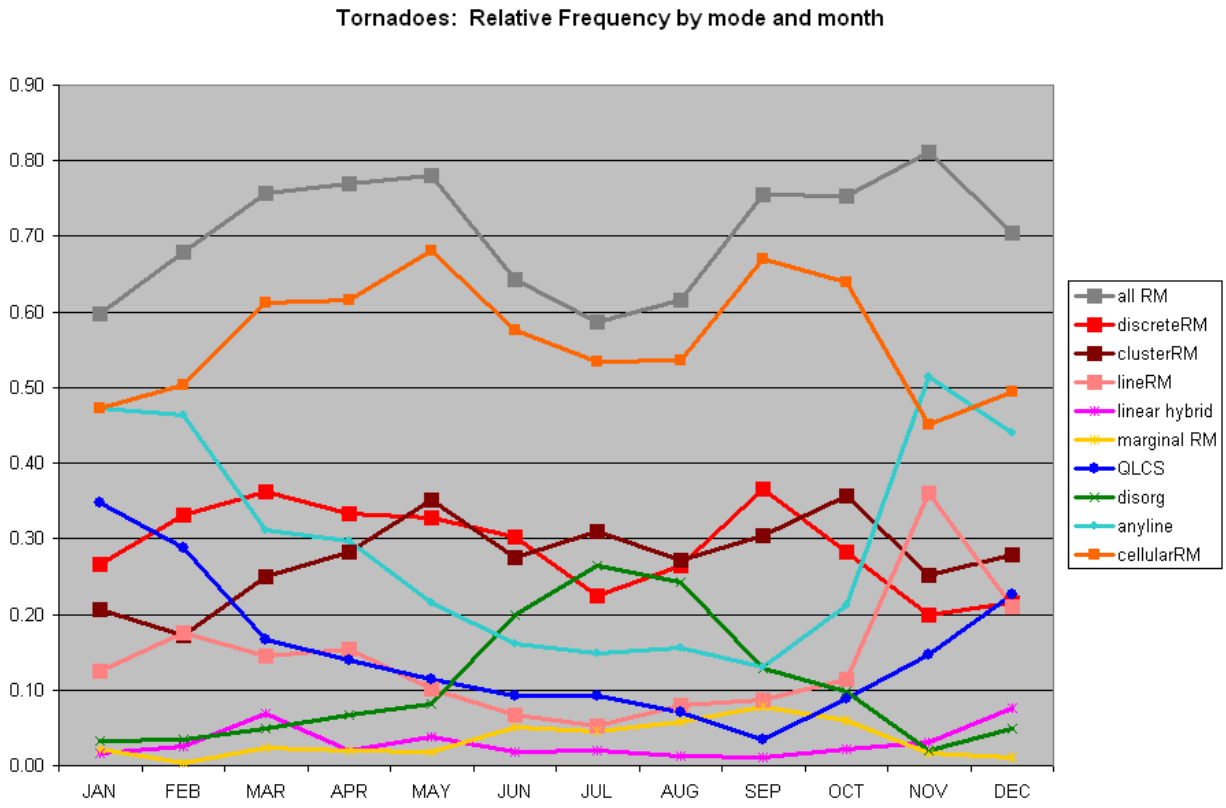

Figure 21. Same as Fig. 20 except for tornado event convective mode relative frequency by month. The "anyline" category includes both QLCS and line RM, and the "cellularRM" category is a combination of discrete and cluster RM.

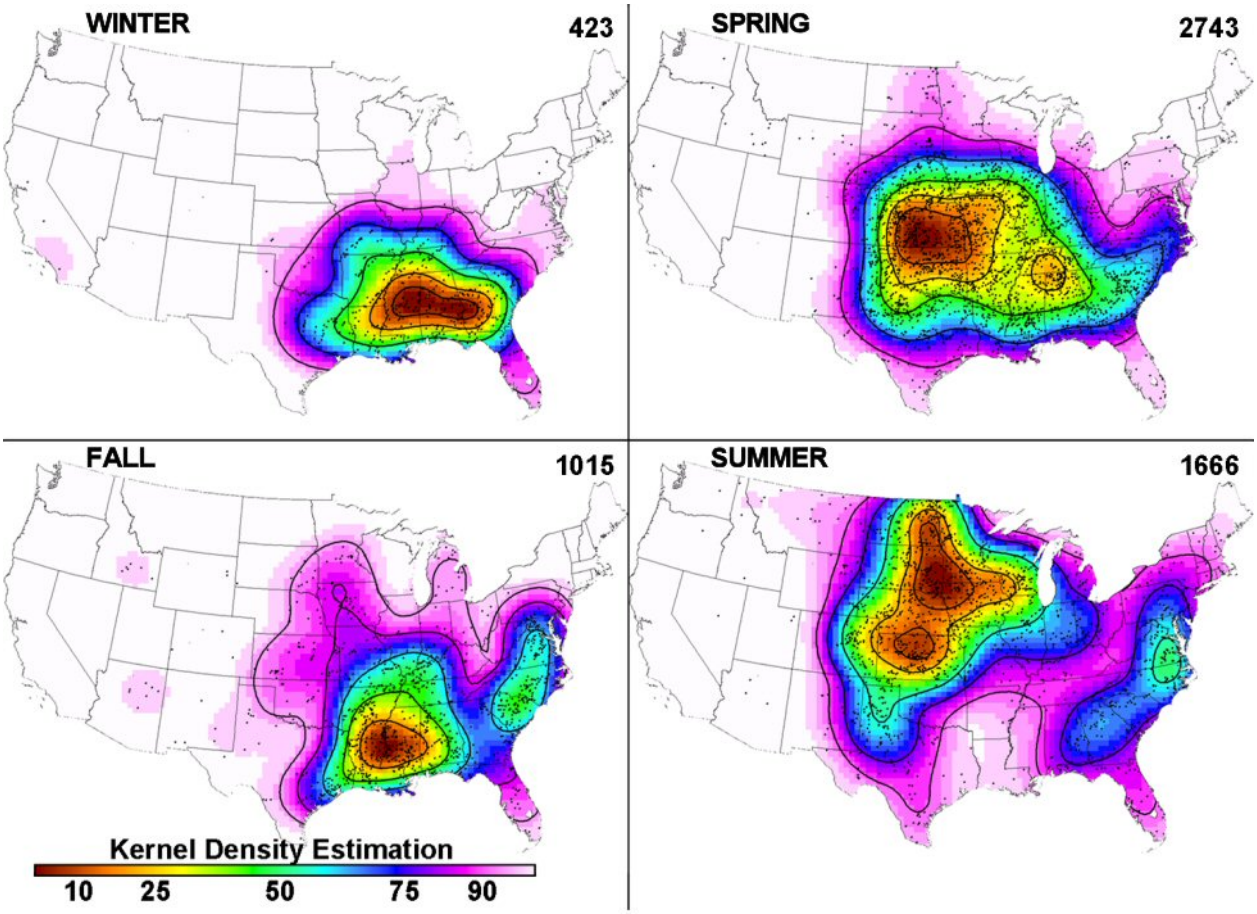

Figure 22. Kernel density estimate on a 40x40 km grid of all RM tornado events by season (top left DEC-FEB (winter), top right MAR-MAY (spring), bottom right JUN-AUG (summer), bottom left SEP-NOV (fall). The outer-most black contour encloses 90% of the kernel density estimate of tornado events, with additional contours at 75%, 50%, 25% and 10%. Black dots represent tornado events (sample size upper right) that formed the basis of the kernel density estimate, and the color-fill legend for density is shown at the lower left.

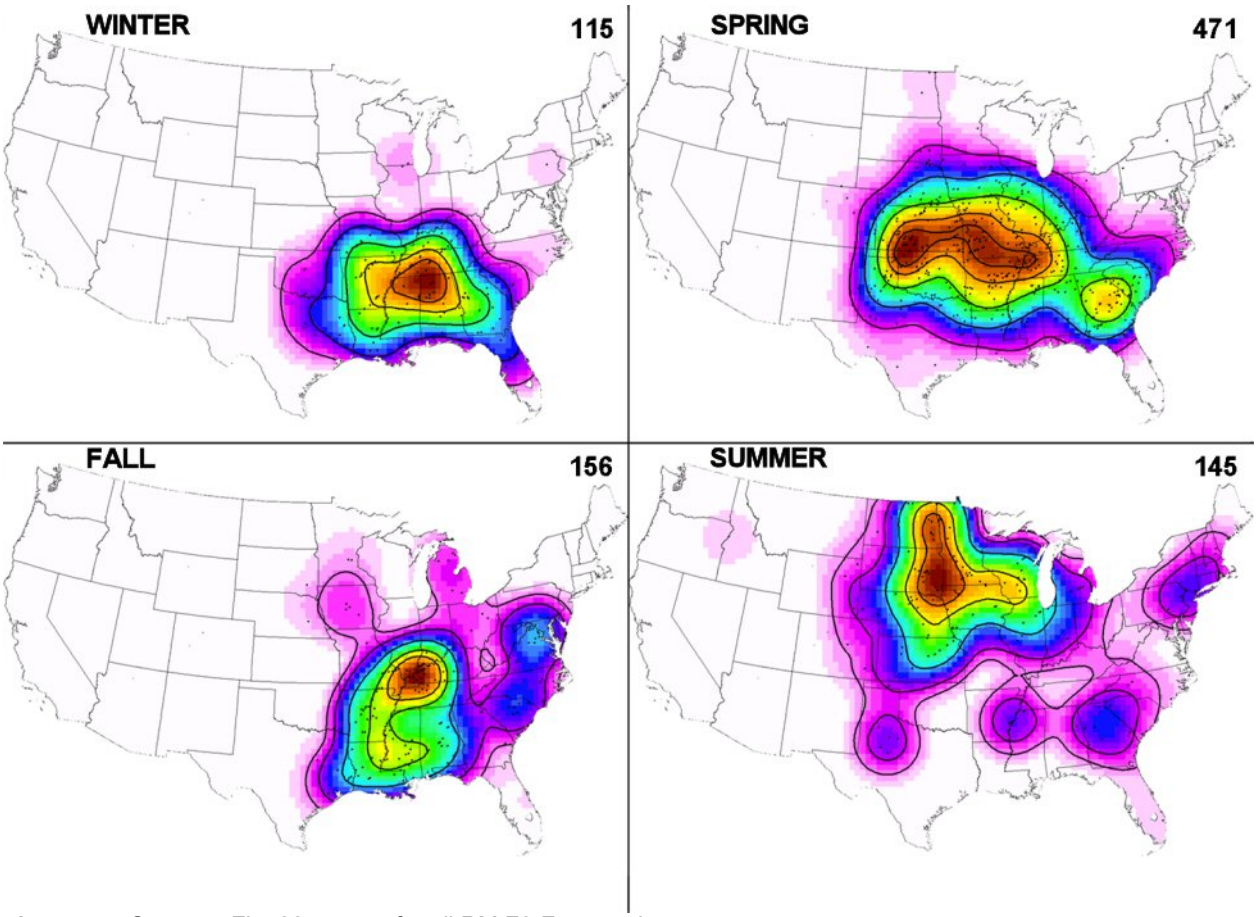

Figure 23. Same as Fig. 22, except for all RM F2-F5 tornado events.

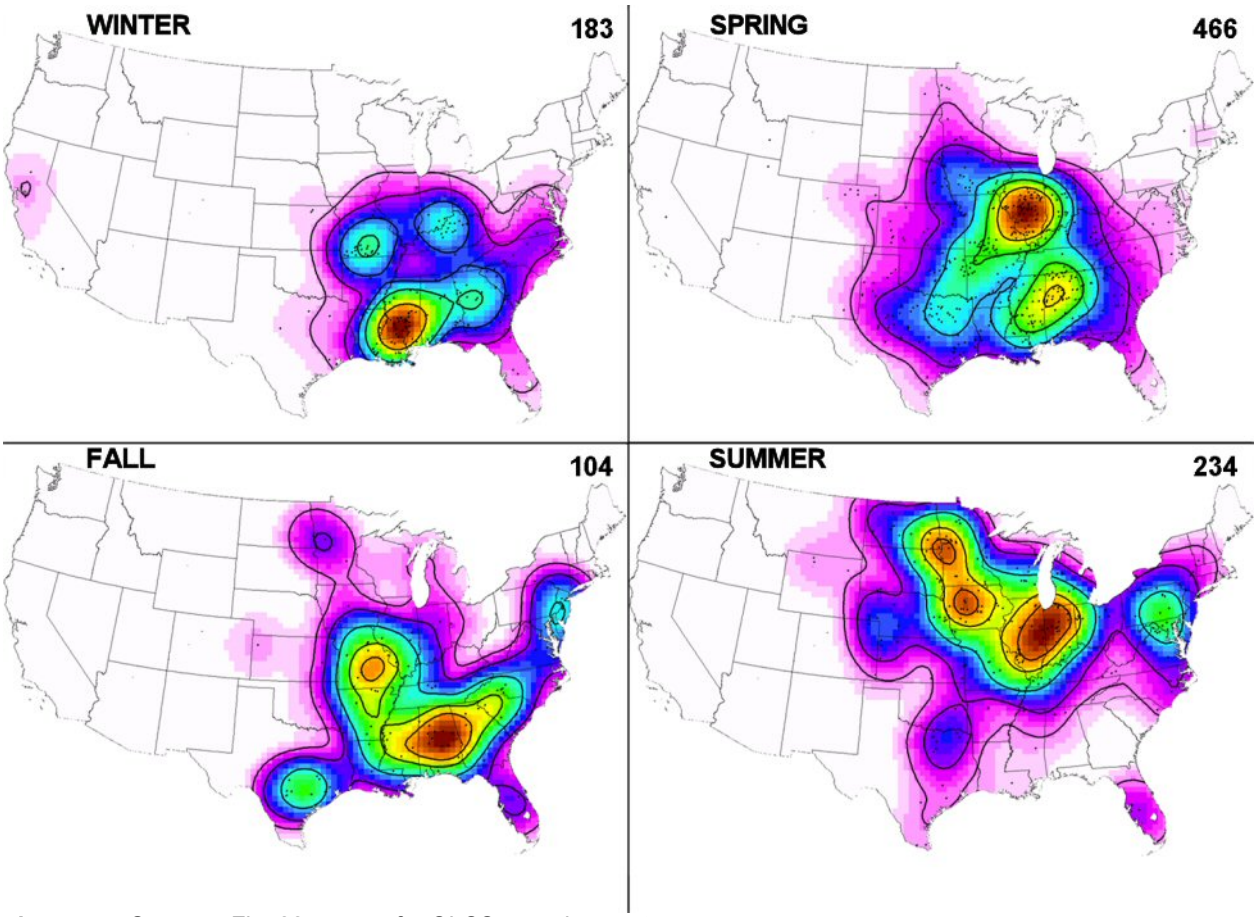

Figure 24. Same as Fig. 22, except for QLCS tornado events.

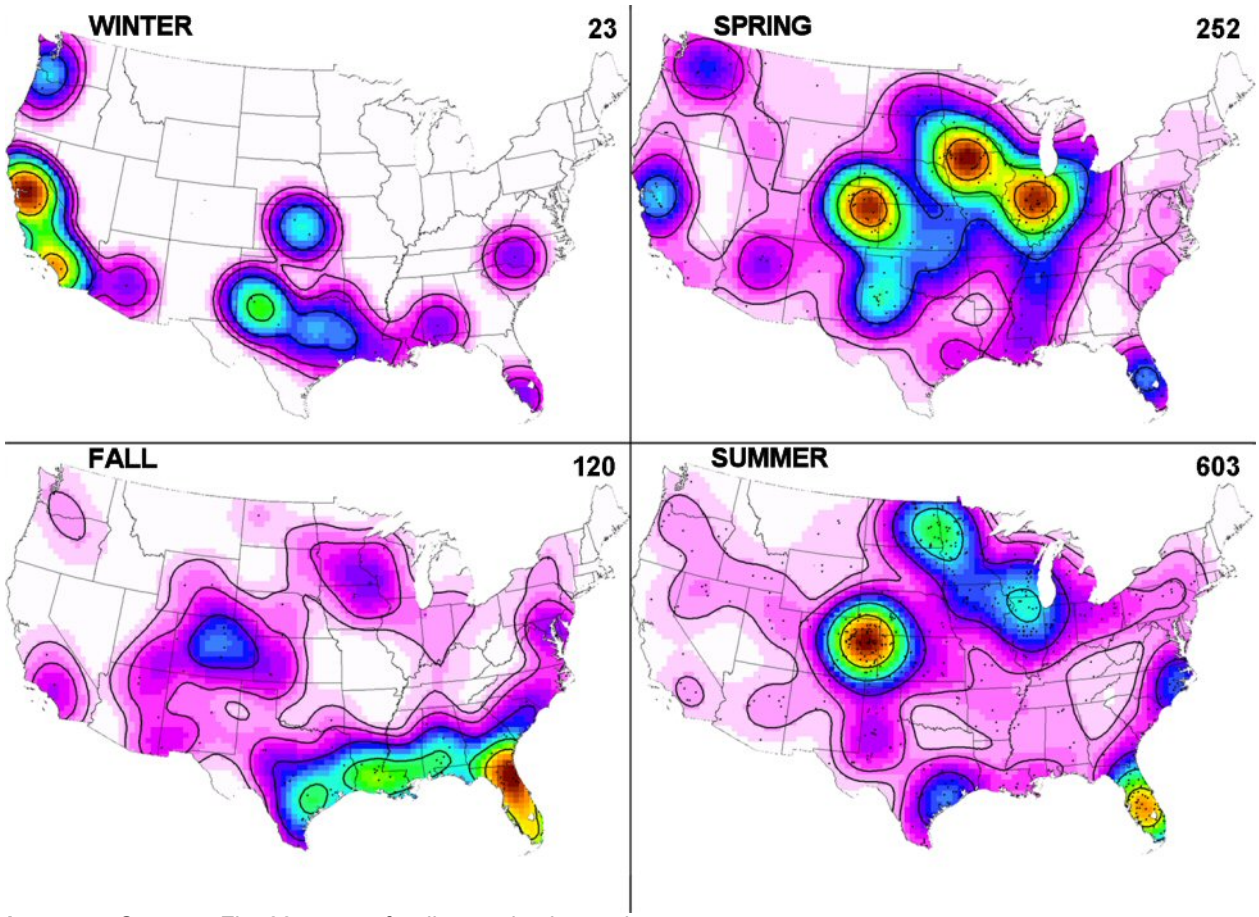

Figure 25. Same as Fig. 22, except for disorganized tornado events.

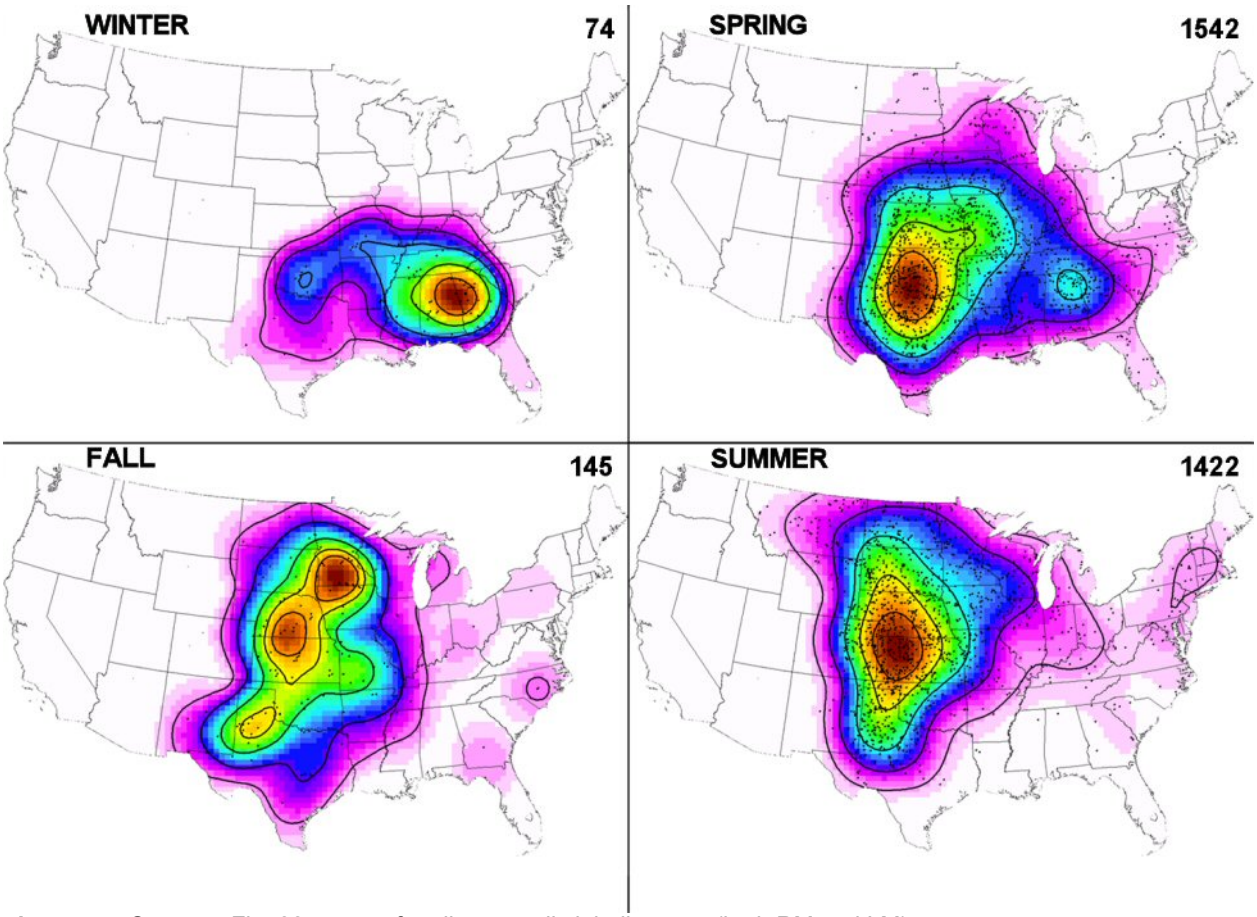

Figure 26. Same as Fig. 22, except for all supercell sighail events (both RM and LM).

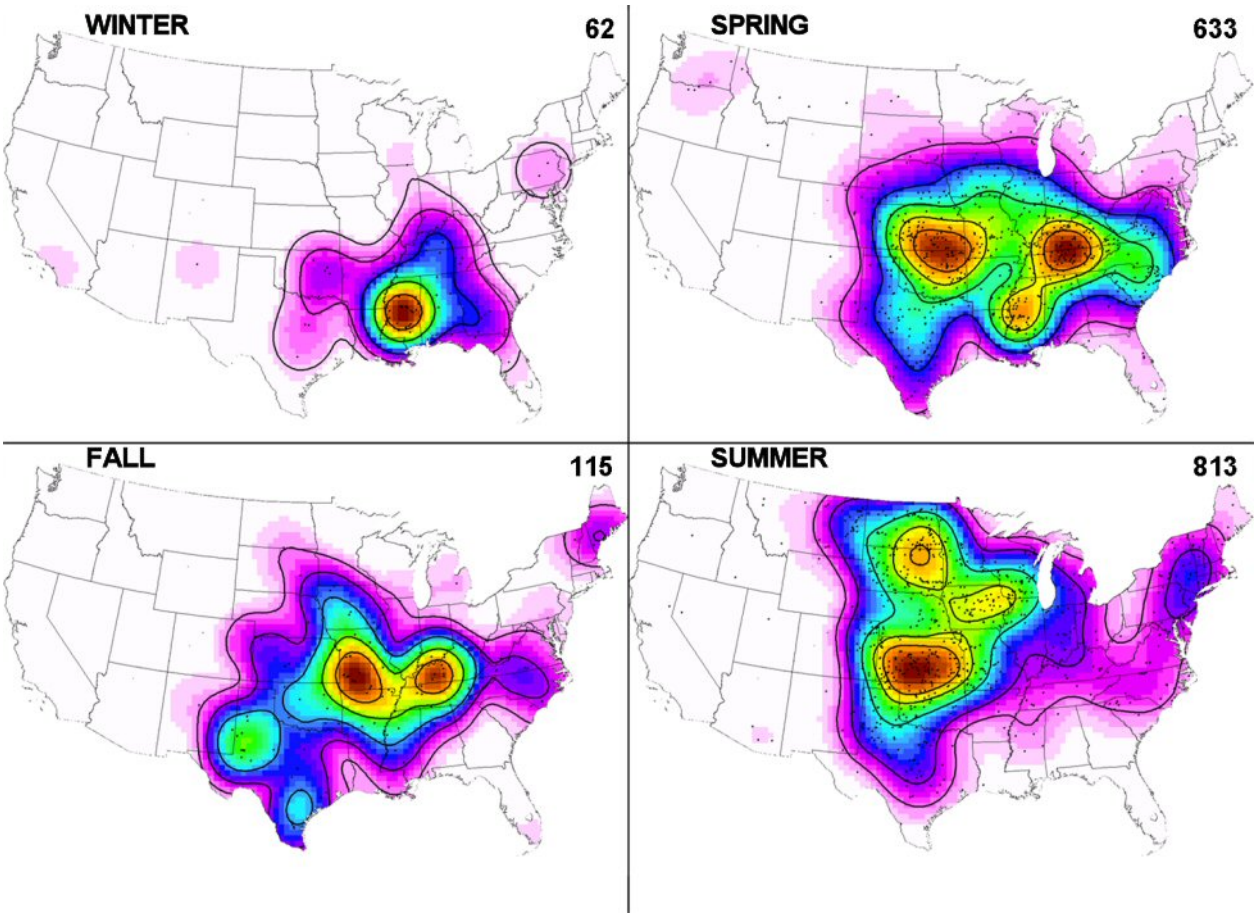

Figure 27. Same as Fig. 22, except for all RM sigwind events.

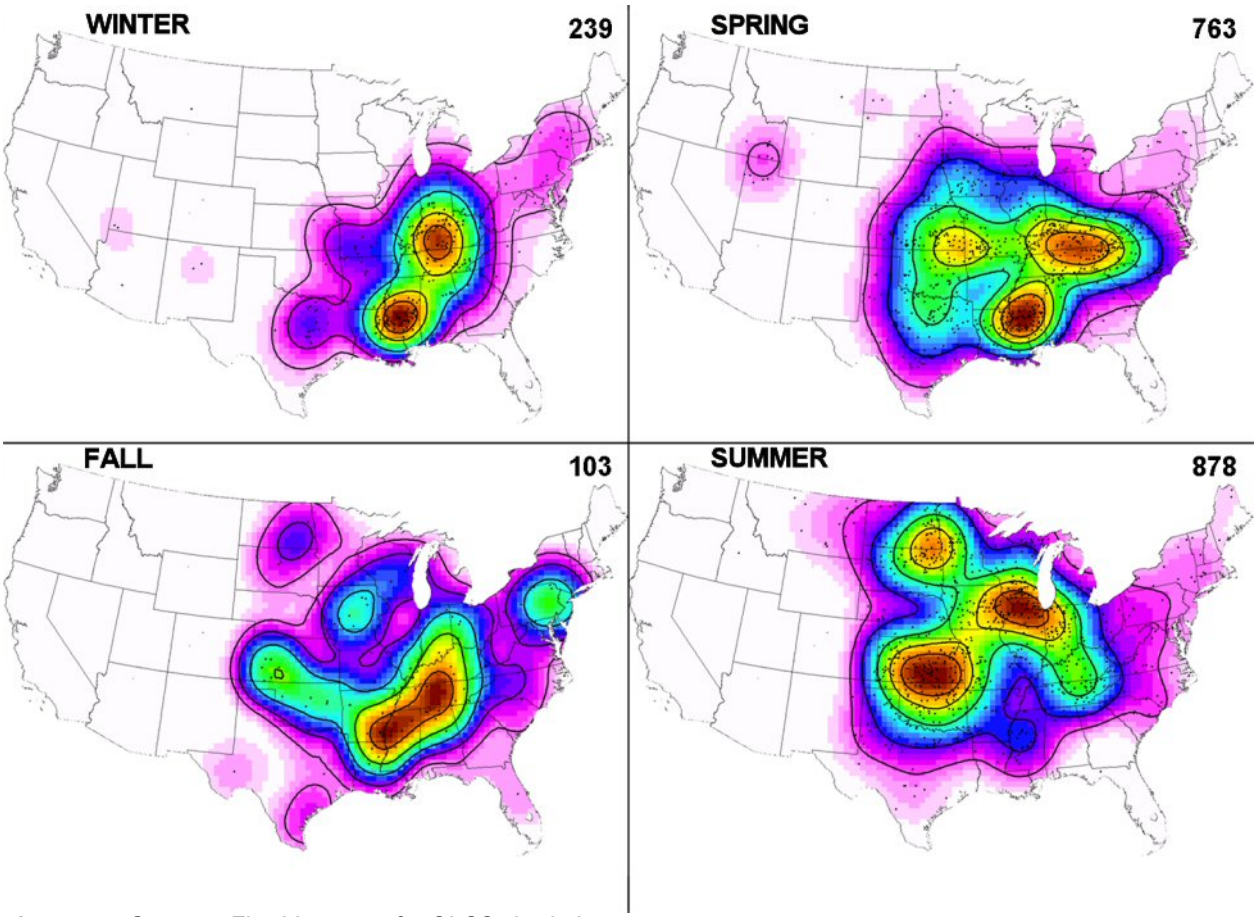

Figure 28. Same as Fig. 22, except for QLCS sigwind events.

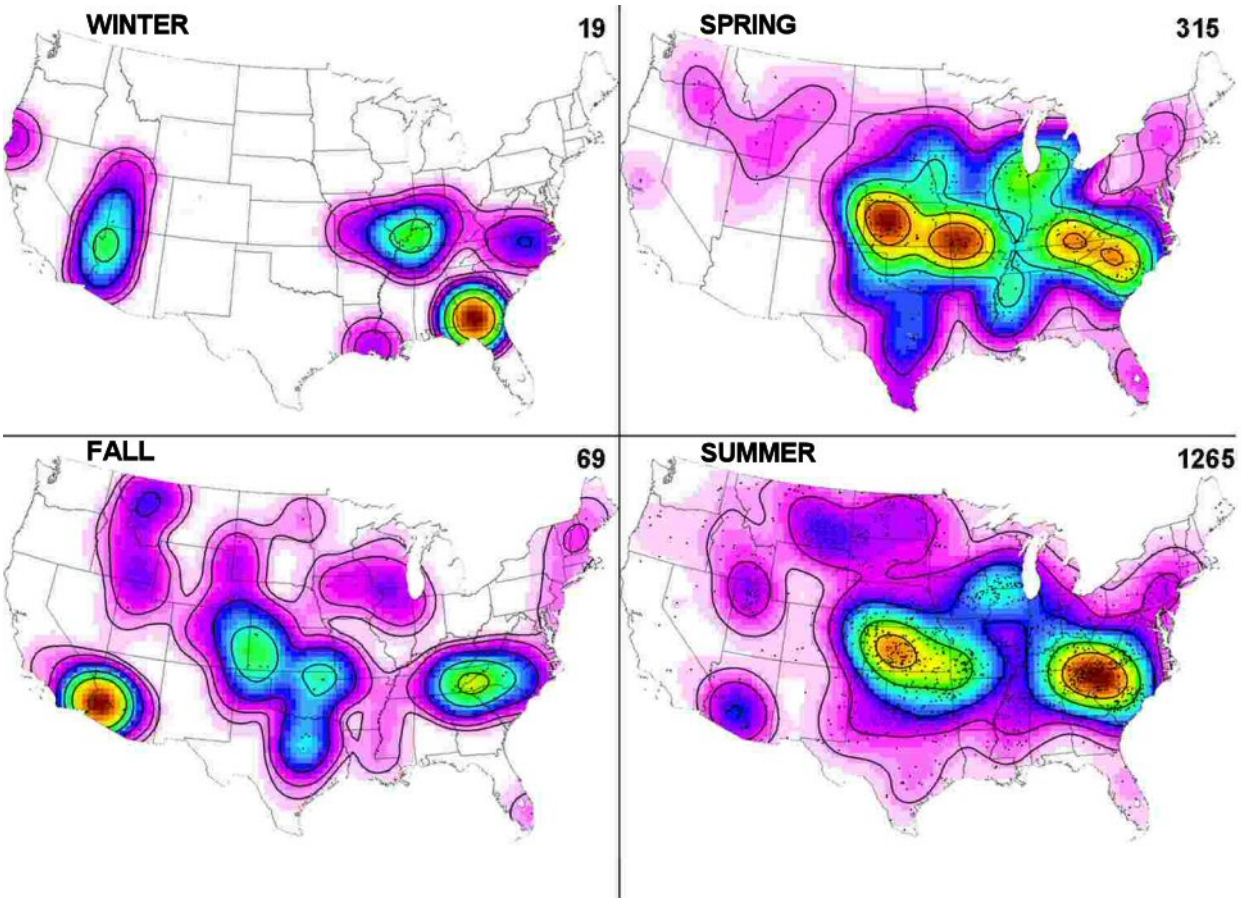

Figure 29. Same as Fig. 22, except for disorganized sigwind events.

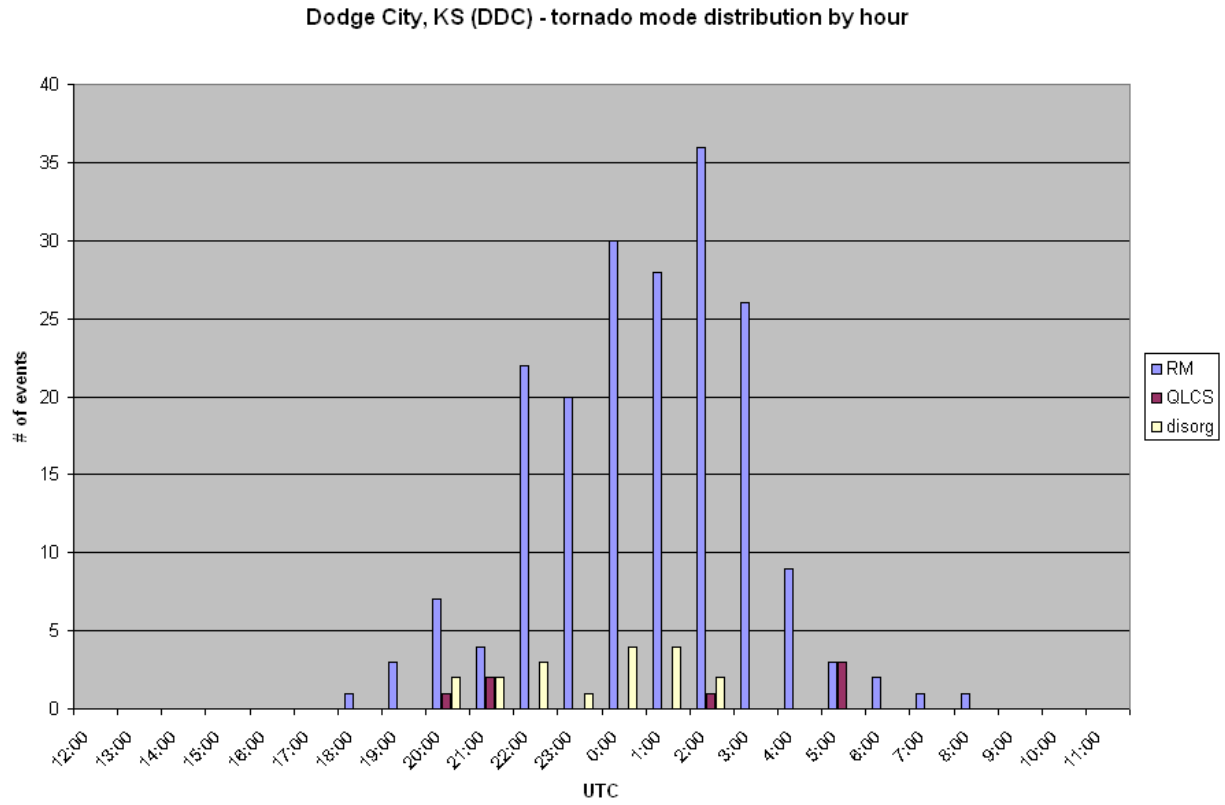

Figure 30. Frequency of tornado events by hour and convective mode, for those closest to the Dodge City, KS WSR-88D site. Events were binned according to the hour of occurrence (e.g., 2045 UTC is listed here as 2000 UTC).

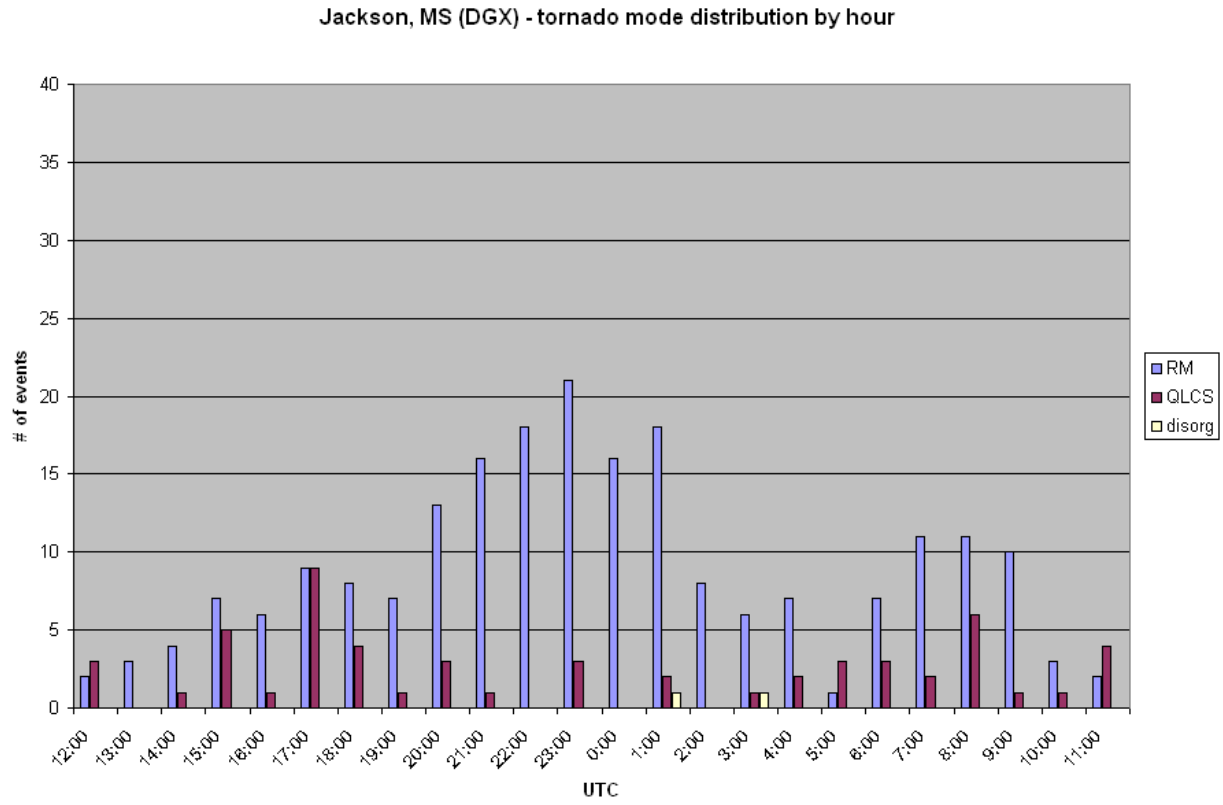

Figure 31. Same as Fig. 30, except for Jackson, MS.